Stony Brook University

Effect of Processing Conditions on the Anelastic Behavior of Plasma Sprayed Thermal Barrier Coatings

A Thesis Presented

by

Vaishak Viswanathan

to

The Graduate School

In Partial Fulfillment of the

Requirements

for the Degree of

Master of Science

in

Materials Science and Engineering

Stony Brook University

December 2011

Stony Brook University

The Graduate School

Vaishak Viswanathan

We, the thesis committee for the above candidate for the
Master of Science degree, hereby recommend
acceptance of this thesis.

Dr. Sanjay Sampath – Thesis Advisor
Professor, Materials Science and Engineering

Dr. Christopher Weyant
Assistant Professor, Materials Science and Engineering

Dr. Toshio Nakamura
Professor, Mechanical Engineering

This thesis is accepted by the Graduate School

Lawrence Martin

Dean of the Graduate School

Abstract of the Thesis

Effect of Processing Conditions on the Anelastic Behavior of Plasma Sprayed Thermal Barrier Coatings

by

Vaishak Viswanathan

Master of Science

in

Materials Science and Engineering

Stony Brook University

2011

Plasma sprayed ceramic materials contain an assortment of micro-structural defects, including pores, cracks, and interfaces arising from the droplet based assemblage of the spray deposition technique. The defective architecture of the deposits introduces a novel "anelastic" response in the coatings comprising of their non-linear and hysteretic stress-strain relationship under mechanical loading. It has been established that this anelasticity can be attributed to the relative movement of the embedded microstructure

under varying stresses. While the non-linear response of the coatings arises from the opening/closure of defects, hysteresis is produced by the frictional sliding among splat surfaces. Recent studies have indicated that anelastic behavior of coatings can be a unique descriptor of their mechanical behavior and related to the micro-structural configuration. In this thesis, a multi-variable study employing systematic processing strategies was conducted to augment the understanding on various aspects of the reported anelastic behavior.

A bi-layer curvature measurement technique was adapted to measure the anelastic properties of plasma sprayed ceramic. The quantification of anelastic parameters was done using a non-linear model proposed by Nakamura et al. An error analysis was conducted on the technique to know the available margins for both experimental as well as computational errors. The error analysis was extended to evaluate its sensitivity towards different coating morphology. For this purpose, three coatings with significantly different microstructures were fabricated via tuning of process parameters. Later the three coatings were also subjected to different strain ranges systematically, in order to understand the origin and evolution of anelasticity on different microstructures. The last segment of this thesis attempts to capture the intricacies on the processing front and tries to evaluate and establish a correlation between them and the anelastic parameters.

Dedicated To
My Parents

Table of Contents

List of Figures

List of Table

Acknowledgements

I would like to convey my special regards to Professor Sanjay Sampath for being extremely supportive as well as for providing guidance all throughout. I would also like to express my sincere gratitude to Professor Nakamura for his expert advice on experiments. I am also thankful to Professor Chris Weyant for agreeing to be a part of my committee

I am extremely grateful to Dr. Gopal Dwivedi for being by my side always and guiding me. I would also like to thank Dr. Kentaro Shinoda, Dr. Yang Tan ,Dr. Brian Choi, Dr. Alfredo Valarezo, Chris Jensen, Travis Wentz, Junghan Kim, Dr.Yikai Chen, Glenn Bancke,Lorena Bejarano, Ling Li, Ravi Dey and all other mebers of the CTSR family. Dr. Jim Quinn of the Materials Science and Engineering Department has been instrumental in providing assistance with microscopy studies.

I am grateful to Debby Michienzi and Chandrani Roy for their help and support with my paper works.

I would like to thank my parents, family, friends and well wishers for their love and support.

1. Introduction

Thermal spray processing technique has been used extensively to create engineered surfaces[1, 2]. The vast application of thermal spray coatings in areas as diverse as gas turbine engines and heavy machinery to as delicate as biomedical implants is a testament to its immense potential. The flexibility with wide range of material selections and the ease of coating deposition on complex geometries makes this processing technique unique to the materials processing society. Thus it has been widely utilized to provide protection to materials exposed to a variety of environments. For example, on one hand while thermally sprayed coatings act as thermal barriers for gas turbine engines[3, 4], they are also used to provide wear resistance and corrosion protection. This thesis, in particular, would be focusing on thermally sprayed ceramic coatings specifically applied to hot section of gas turbine engines. With the advancements in gas turbine engines' technology its various components are being subjected to harsher environments and the demand of higher operating temperature presents significant increase in challenged on materials durability This thesis is an attempt to examine, investigate and understand some of the key issues related with current plasma sprayed TBCs focusing majorly on their mechanical properties.

The application of TBCs enables the engines to continue operating at higher temperatures (for better efficiency) without running the risk of damaging the base material [5] A TBC consists of a thin layer of ceramic topcoat which is deposited on the

metallic substrate. The ceramic being used in the industry at present is 6-8 wt% Yttria Stabilized Zirconia (YSZ). This material has been chosen and accepted by industry standards due to its low thermal conductivity, resistance to thermal fatigue and good thermal and chemical stability[6]. Such ceramic coatings are deposited either using plasma spraying technique or electron beam physical vapor deposition (EBPVD). Both these techniques produce distinctively different coating architectures due to the difference in the coating deposition principle. While the EBPVD produces a vertical columnar grain structure, plasma spray produces a flat pan cake shaped layered structures. Both these coating deposition techniques have their own pros and cons. Our focus would be on plasma sprayed TBCs[7].

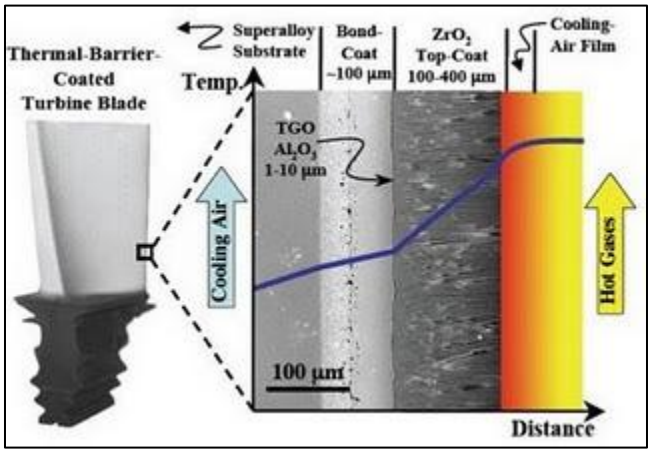

Figure 1-1: Thermal barrier coating on a turbine blade processed using EBPVD process[8]

In general, a thermal spraying technique has two major components to it: one is the thermal energy that is needed to melt the particles, and the second one is the kinetic energy required to direct the molten particles towards the surface being coated. The source of thermal energy can be electric arc or combustion fame. Particular to our interest here, in Atmospheric Plasma Spraying (APS), the heat source (gas plasma) is

generated by an electric arc method[9]. This consists of an anode and cathode which are usually made of copper and tungsten respectively. The material in the form of powder, carried by an inert gas such as He, is subjected to the plasma plume where it gets molten and accelerated in the plume. When these molten droplets come in contact with the substrate they undergo rapid quenching (quenching rate 10^{-6} K/sec)[10]. The surface of the droplet which comes in contact with the substrate begins cooling[11]. As a result the solidification of the droplet starts from that region, and an interface is thus formed which would demarcate the solidified and the molten zones of the particle. As time goes by the interface, also referred to as solidification front, begins to move upwards indicating the solidification of the entire molten particle. Ultimately the particle is deposited on the surface and is now referred to as a "splat". As more and more particles arrive on the surface they deposit on a previously deposited splat or substrate. They undergo similar mechanisms as explained above. Due to this layer-by-layer deposition of particles thermal spray process tends to generate a lot of interfaces.

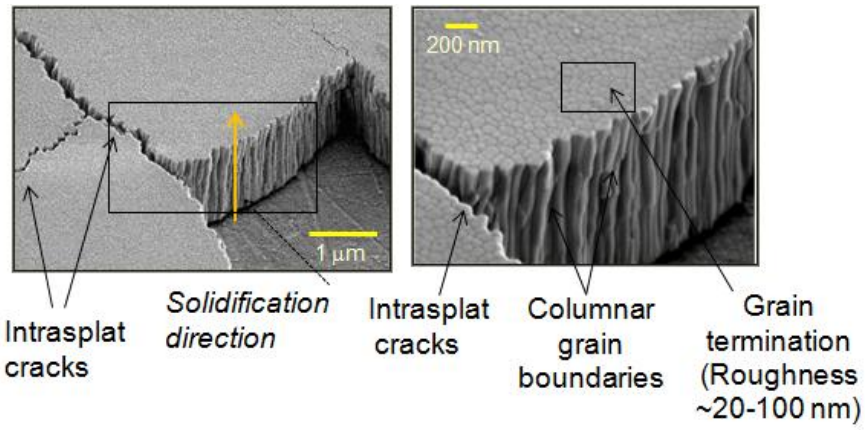

Figure 1-2: SEM image of splat solidification and defect formation in a plasma sprayed YSZ coating [12]

Figure 1-2 shows SEM micrographs of a YSZ splat on a smooth metallic surface. It can easily visualized that the columnar grains nucleate at the substrate-splat interface and continue to grow away from the substrate[10]. The columnar grains provide an additional grain boundary interface which may have some influence on the material properties. Figure 1-2 also shows the existence of mud-cracks within a splat which are attributed to release in stresses during or at the end of solidification process. This is generally true for a crystalline ceramic material. In addition, it is important to notice that at the end of solidification process, the grain termination sites provide a rough splat surface (20-100 nm). All these defect surfaces may play a significant role on coating properties. We will discuss and elaborate more on this later.

1.1. Plasma spray process

In order to understand the coating deposition process, it is important to know the actual deposition process. Figure 1-3 shows the schematic of a plasma spray system. The enclosure within which the combustion of the gases takes place is referred to as a "gun" or a "torch". Usually gases such as hydrogen are used. Due to the combustion of the gas a flame is produced. The momentum and heat for the particles is provided by this combustion flame or thermal plasma[13]. This is the source of thermal energy and is referred to as "plume". Various parameters in the processing can be modified to control the enthalpy as well as kinetic energy of the plume to bring about changes in the coating microstructure[14]. The material to be coated is fed into hoppers and is fed into the injector line. The schematic shown here is that of an external injection. This means that the powder is injected into the plasma plume outside the nozzle. As seen in the schematic, the plume may not of a uniform dimension throughout. The position of the injected particle in the plume has a lot of influence on the particle's melting index. The

particle travels through the plume and the duration that it remains in the plume is referred to as "dwell time". Increase in particle dwell time ensures better melting of the particles. However, an excess dwelling may cause material evaporation. Each individual flattened and solidified particle is referred to as *"splat"* and this is the basis of any thermal spray microstructure[15].

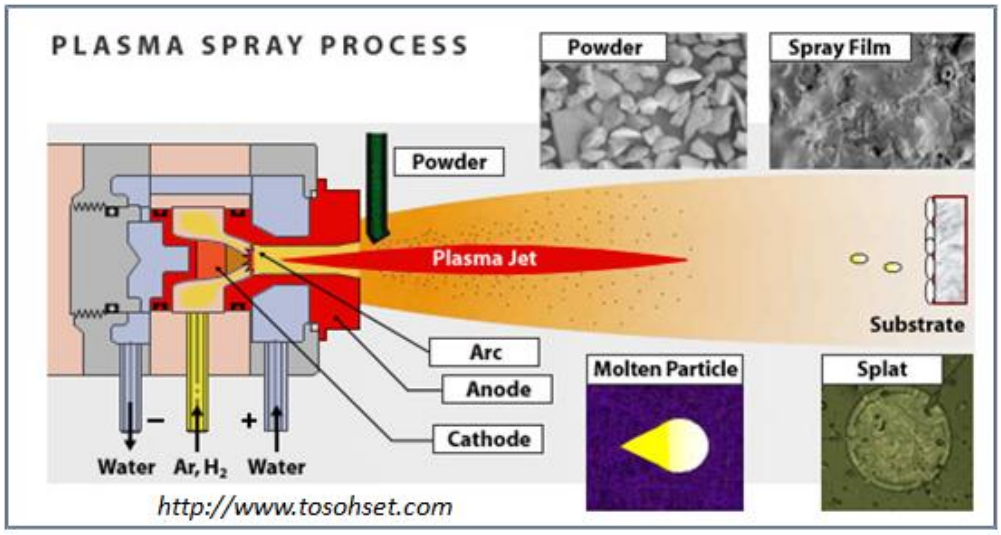

Figure 1-3: Schematic of a plasma spray process showing the various components of the system. The particles after getting molten in the plume deposit on the substrate as splats[12]

The actual sequence of events in the coating deposition is significantly intricate and involves a lot of phenomenon at the microscopic scale. Therefore, to understand it better, the complete deposition process can be divided into many stages. The evolution of the coating microstructure can be broken down into following stages as shown in the Figure 1-4.

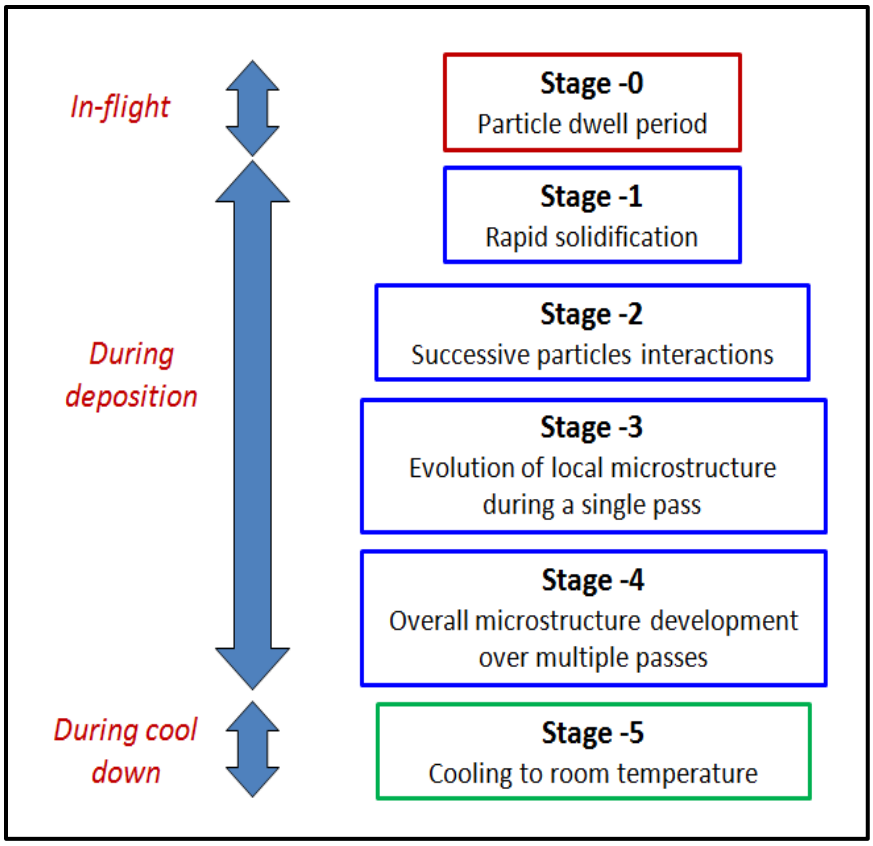

Figure 1-4: The various stages in the evolution of coating microstructure starting from powder injection to the cool down of the coating after deposition. Each of these stages has a significant influence on the final microstructure of the coating

Changes in the melting state of the particle can be brought by changing the enthalpy of the plasma, which can be done by regulating plasma parameters and spray distance. While, plasma parameters can be tuned to control the enthalpy transfer from plasma to particles, the spray distance can decide the particle dwell time in plasma plume. In addition, another deciding factor for particle melting and kinetic energy state is powder morphology and its distribution. Smaller particles would get molten faster than bigger particle. One morphology, for example a fused and crushed (F&C) powder may not acquire same melting state as compared to particle with hollow sphere morphology[16].

Figure 1-5 shows the SEM micrographs of the two different morphologies and of the coatings sprayed using these powder morphologies

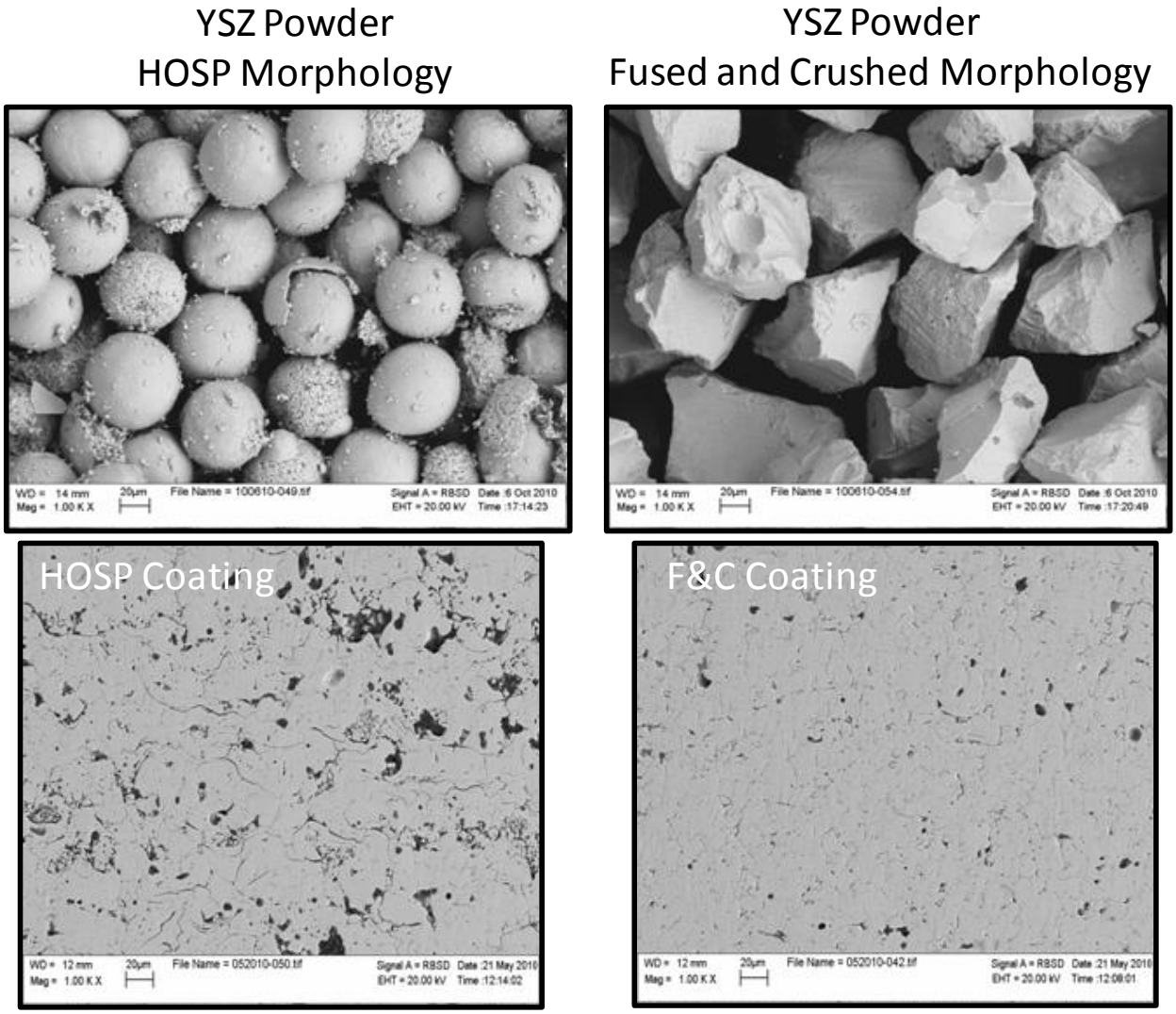

Figure 1-5: Comparison of feedstock powder morphologies (HOSP and F&C) as well as the coatings produced using the two morphology powders. The HOSP powder produces higher defect density as compared to F&C powder

The reason behind higher defect density in coating sprayed using HOSP powder can be attributed to the hollow sphere nature of the powders. This powder is designed to produce coatings with high defect density required for TBCs application.

The kinetic energy of the particles is also a major governing factor. When particles are accelerated with a higher velocity, their dwell time in the plume decreases. This results in decreased melting of the particles thereby once again affecting the overall porosity of the coating. In addition, the injection of the particles in the plume also influences the repeatability of the coatings. The spray process parameters define and control the deposit formation mechanics as well as the resulting microstructure and coating properties. For a given feed rate of the powder one can obtain different coating properties by varying the carrier gas flow. Let us consider the situation where the carrier gas flow is either too low or too high. Under both conditions the particles do not enter the plume the way they should. Under very low carrier gas flow scenario the particles do not enter the plume deep enough. This means that the entire enthalpy of the plume is not being utilized during the coating deposition. On the other hand if the carrier gas flow is too high, then the particles flow all the way through the depth of the plume too soon. In this case though the particles do traverse through the entire depth of the plasma the particle melting would not be optimum. The aforementioned scenarios are known as under injection and over injection of the particles respectively. In order to achieve the optimum injection the particles should enter the plume at a fairly good velocity, they must remain within the depth of the plume during their dwell time. Under such conditions the particles tend to have the maximum temperature and velocity which in turn results in better deposition efficiencies[17, 18]. This ensures that the enthalpy of the plasma is being used efficiently and also greatly enhances coatings'

repeatability. This procedure is termed as injection optimization. The state of particle at the end of "stage 0" is the foundation of further coating deposition.

The "stage-1" where the molten particle comes in contact with substrate material is strongly dependent on substrate conditions. The surface on which the molten particles would deposit greatly influences the final coating architecture. The two parameters which tend to control this are the substrate temperature and roughness. When a molten splat comes in contact with a substrate, the substrate acts like a heat sink. The quenching followed by the solidification of the particles takes place on the substrate. Hence the temperature of the substrate controls the solidification and grain growth mechanism. The splats thus formed undergo bonding with the substrate by mechanical locking. This is governed solely by the roughness of the surface. During the cooling the splats undergo solidification under a constrained volume. This generates a lot of tensile stresses in them[19]. As more and more splats deposit, the stresses build up within the entire coating. Being a layered system the cumulative effects of the stresses build up and impart an overall residual stress state for the coating. Theses stresses manifest themselves in the form of numerous micro cracks in the coating. Though at first this might not seem to be desirable, fact remains that it is the presence of such defects which lends the coating its compliance and decreased thermal conductivity.

1.2. Defects in a plasma sprayed TBCs

Since TBCs face the brunt of the harsh environments in gas turbines and diesel engine's [20] combustion chamber they undergo degradation over a period of time. The lifetime of these coatings and their reliability are key issues to be dealt with. Hence predicting coating life is extremely important. The failure of TBCs usually occurs due to

various phenomena which occur within its microstructure. Various conventional techniques carry out destructive testing, metallographic approaches as well as image analysis to understand the behavior of coating microstructures to predict the coating life. Microscopic defects which are key feature of any TBC play a pivotal role in dictating the coating properties, behavior and thereby its life. An in depth understanding of these defect mechanisms would help tailor the coatings and make them better equipped to face the harsh conditions during the service life. The most prominent types of defects in a plasma sprayed YSZ coating have been show in the figure below.

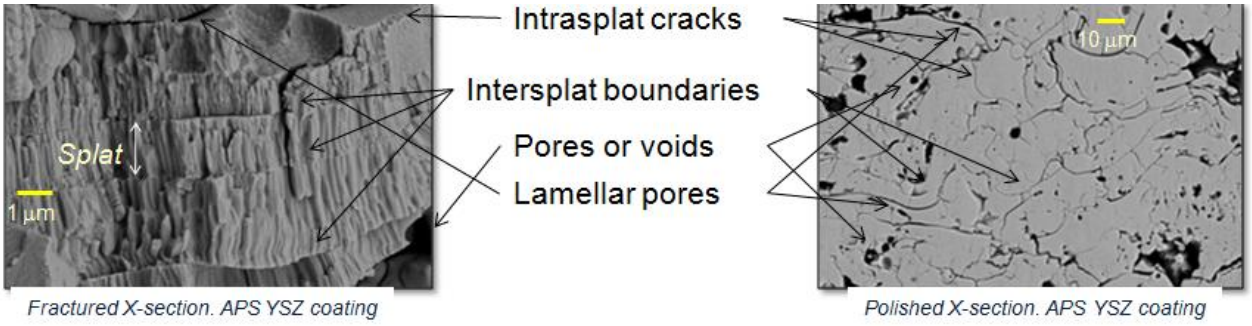

Figure 1-6: The various types of defects in a plasma sprayed YSZ coating observed from SEM imaging. All the features can be observed in both fracture surface as well as polished cross section of the coating

The successive impingement of molten particles leads the deposit to a layered architecture. The interfaces among splats are one of the key features of sprayed deposit. The deposition of a molten particle on a cooled any solidified splat would result in an interface being created at interface, referred to as splat interfaces. Additionally, the layer by layer depositions provides additional interfaces between layers. The nature and morphology of these interfaces play a significant role in the coating's mechanical and thermal behavior. Creation of these interfaces is inevitable. However the thermal spray

society has been successfully utilizing the characteristics of these defects to achieve certain coating properties which are difficult to acquire via bulk materials. For instance a plasma sprayed YSZ coating has a much lower elastic modulus as compared to a bulk YSZ. This reduction in modulus is due to the presence of the numerous defects in plasma sprayed YSZ which lends the YSZ lower thermal conductivity and enhanced fracture toughness. Majority of their attributes can be controlled by controlling the processing conditions[21].

Since an interface can be treated as two surfaces in contact, its roughness is one of the parameters which could have a telling effect on the coating's properties. Usually coatings tend to undergo a lot of mechanical stresses during their service life. Under such circumstances these interfaces tend to slide to and fro and this is when the roughness of the interface contributes to the behavior of the coating.

In addition to the splat interfaces, there are other defects which are present in a plasma sprayed TBC, which can have influence on coating properties[22]. Most of these defects, including splat interfaces, get formed during deposition; however some of the micro cracks can be introduced during the post-deposition cool down process. As mentioned earlier, the rapid quenching of molten particle during deposition develops a high tensile quenching stresses in the coating, a part of which can be released by adapting cracking phenomenon. As more and more material is being deposited the stresses in the coating build up during the cooling of the system. Beyond a certain point there arises a need for the system to relieve itself of stresses. Ceramics being brittle cannot undergo plastic deformation. Hence the manner in which the stresses get relieved is by the creation of micro-cracks in the coating. Thus in a plasma sprayed coating cracks are inherently present as a result of the conditions under which the coatings are formed. These cracks have a crucial role to play during the service life of a

TBC. Since the nucleation of the cracks have already taken place during coating deposition, their propagation/blunting during thermal cycling are critical. In a densely packed coating, it is possible that the cracks tend to coalesce relatively easily when compared to a more porous coating. This is because in a porous coating the presence of pores tends to inhibit the crack propagation. In addition, at the end of deposition, the coating is in tensile stress state and during the cool down the coating-substrate system undergo under compression leading the coating to a relatively lower tensile or compressive stress state at room temperature. This compressive stresses imparted on a deposited coating during cool down majorly depends on the mismatch of coefficient of thermal expansion mismatch between coating and substrate, deposition temperature and the stiffness of deposit. This cool down process may introduce additional cracking to the deposit structure[23]. Since the properties of a coating are prescribed by its defect density, understanding the influence of the crack density and morphology on properties will help tailor the coatings to meet specific requirements[24].

Pores are formed due to the spacing that is created during the splat formation. If the adhesion between two successive splats is not good enough then they create pores in between them .Pores can also be created around an un-molten particle in a fully molten matrix. Just like the other defects, pores also play their part in governing coating properties. The presence of pores tends to dissipate the energy of phonons during thermal exposure. As a result they decrease the through thickness thermal conductivity of the coating, which is a desirable for TBCs.

1.3. Anelasticity in plasma sprayed YSZ

The TBCs applied to most of the hot sections of gas turbine engines experience a significant amount of stress change during ramping up as well as the cool down of the engine. Though during both the operations the engine is subjected to significant levels of stress, it is the cool down stage which is prone to cause more damage due to the higher rates of stress generation[25]. The plasma sprayed TBCs coatings have been showing promise in accommodating such large stress changes due to their strain tolerant nature originating from the defective architecture of sprayed coatings. The strain tolerance, also referred as coating compliance, of these structures not only provides adequate flexibility to coating accommodate high strains, it is also useful for providing strength to withstand centrifugal loads.

Recent observation has shown that these coatings, under mechanical loading shows, not only non-linear behavior but also hysteretic response, collectively named as anelastic behavior of the coating[16, 26-29].Of our interest in this thesis, the thermo mechanical response of TBCs sprayed on a planar substrate is shown in figure 7. As it can be observed, the curvature-temperature response of the coating-substrate bi-layer system is non-linear as well as hysteretic.

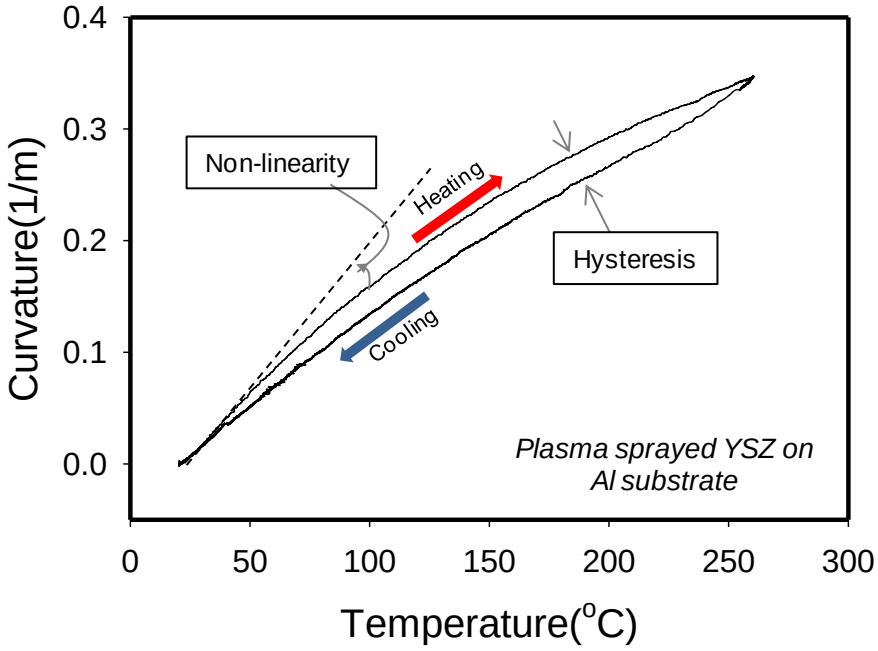

Figure 1-7: Nonlinearity and hysteresis in a plasma sprayed YSZ coating when subjected to thermal loading[12]

The proposed mechanisms explaining these unique behaviors are not yet very well defined however based on past research it can be summarized that the overall anelasticity is a defect architecture driven phenomenon[16, 28]. The nonlinearity, deviation from linear behavior, was due to the presence of the pores and relatively wide open interfaces in the coating. On the other hand the hysteresis part of anelasticity originates from frictional sliding at interfaces which changes with applied stress.

In the case of our coating substrate (YSZ-Al) system, coatings are in significantly compressive high stresses at room temperature. Under such conditions many cracks in the coating are closed. Upon thermal cycling the stresses shift towards towards the tensile regime and consequentially the crack faces open up. Since the coating becomes more compliant with the crack opening, the effective strain increases. Such opening and

closing of cracks have been illustrated in Figure 1-8. The effect of pores on coating's nonlinearity is also significant, though the porosity majorly contributes to the reduction in the overall elastic modulus of the coating.

In addition to nonlinearity the response of the coating to thermal loading is hysteretic as well. The responsible mechanism behind such a behavior is the frictional sliding at interfaces and crack surfaces. The straining in the coating causes dissipation of frictional energy during a thermal cycle. Such a release of energy upon frictional sliding causes the hysteretic behavior of the coatings [12].

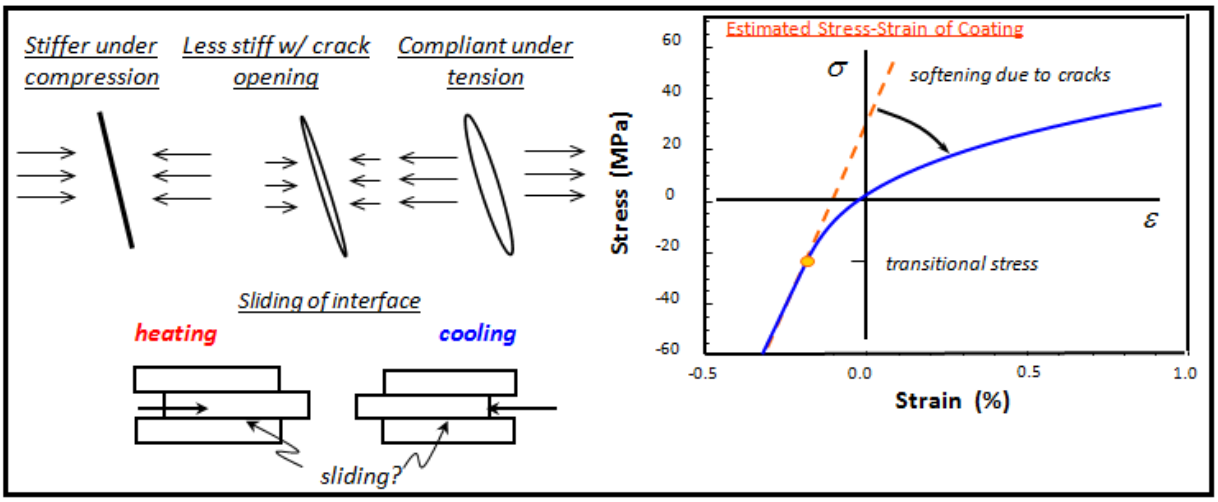

Figure 1-8: Illustration of the origin of Nonlinearity and Hysteresis in plasma sprayed YSZ. Schematic shows the opening /closing of crack as well as the sliding of the splat interfaces. The resulting compliance in the coating is evident in stress-strain response of the system[12]

Since every coating has its own defect architecture its anelastic properties are also unique to itself. This uniqueness of anelasticity for each coating allows one to treat anelasticity as a coating signature. Although one cannot replicate exactly same defect architecture in two different coatings, it is possible to achieve similar microstructure to

what is desired and hence the signature. This thesis utilizes this concept of anelasticity to explore the control of nonlinearity and hysteresis from the processing end[27]. If a correlation could be established between the anelastic parameters and processing parameters, it would help us to better tailor the defect architecture so that they can be better equipped to take on the challenges which the next generation of turbines hurls at them.

2. Statement of Problem

Thermal barrier coatings (TBCs) applied to the turbine blades in gas turbine engines are subject to not only thermal loads but also to mechanical loads due to the motion of the blades as well as the thermal mismatch stresses. Therefore, in addition to low thermal conductivity required to provide adequate thermal barrier, a good mechanical compliance is also desired for the longevity of the coatings. In general, the defect distribution in plasma sprayed YSZ tackles both these issues quite elegantly. The plasma spray process used for TBCs deposition intrinsically introduces numerous defects to the coatings due to nature of the process. It has been well established that the presence of these microscopic defects in a coating plays a significant role in the overall performance of the coating. These defects comprising of cracks, lamellar and globular pores and splat interfaces tend to undergo certain changes at the microscopic level when subjected to thermal or mechanical loading. The crack faces tend to open and close while the splat interfaces tend to slide to and fro depending on the stress state. Due to such a dynamic nature of the coating system, their stress strain response is non-linear exhibiting the strain compliant nature of the coatings. In order to understand the exact role of these defects on coating performance, it is important to understand the response of these defects in terms of their non-linear property via certain systematic changes brought about in the processing conditions.

The measurement of the nonlinear parameters is carried out using the advanced bi-layer curvature measurement technique. When a coating – substrate system is subjected

to temperature change the thermal expansion mismatch between them manifests itself in the form of change in overall curvature of the bi-layer system. This response could be exploited to extract the nonlinear stress-strain behavior of the coatings. Furthermore based on the numerical model developed by Nakamura and co-workers, the non-linearity can be quantified based on the low temperature linear elastic modulus of the coating (E) as well as the non-linear degree (ND). The parameter ND gives an estimate on the extent to which the coating has deviated from its linear mechanical response. This information in turn could be used to shed light on the defect density present in a coating.

With a hypothesis of anelastic behavior being governed by the density, orientation and distribution of cracks and pores present in a coating, this thesis focuses on the micro structural sensitivity of anelasticity along with changes in process parameters. In order to avoid any erroneous interpretation of data, analysis was conducted on a single specimen with introduction of some possible human errors to investigate fidelity of the anelastic parameters. Later, the extent of repeatability of coatings' anelasticity with respect to defect density was examined by analyzing multiple specimens prepared at three different processing conditions.

It is also essential to understand the temperature dependency and consequentially the strain range dependency of anelastic parameters. Chapter seven discusses the outcome of such analysis. Lastly, based on a systematic experimental design, an effort was made to establish a correlation between anelastic parameters and some of the process parameters such as powder feed rate, spray distance and torch traverse speed. The results suggested that with changes in the processing conditions the defect architecture of the coatings varied significantly and these were reflected on their computed non-linear parameters.

3. Experimental Procedures

3.1. Plasma torch

The torch used for plasma spraying consists of two water cooled electrodes namely the anode and the cathode between which a stable arc is generated using a current source. Vortex plasma was generated using Sulzer Metco's F4 H2 torch. Inert gases such as Ar and Nitrogen are used to control the trajectory of the particles in the plume while hydrogen gas is used to control the enthalpy of the plasma. For lower energy condition the hydrogen flow rate is decreased. The compositions of the gases are changed depending on the required coating conditions. The gases get ignited inside the torch and the generated plasma comes out of the torch by the virtue of the carrier gases.

3.2. Powder feeding

The powder is fed using Technik Twin 10 feeder externally. The carrier gases (He) carry the powder into the plume and then towards the substrate. The manner in which the particles are carried by the carrier gases plays a major role in the temperature and velocity of the particles in the plume. At very low carrier gas flow rates the particles are said to be under injected and at very high flow rates than that is desirable, the particles are said to be over injected. Thus an optimum carrier gas flow rate is essential for the proper injection of the powder into the plume. This technique is known as injection optimization. The effect of injection optimization has briefly been discussed in the first chapter.

3.3. Particle diagnostics

The flow of particles in the plume is monitored using two sensors DPV2000 and AccuraSpray g3 (Tecnar Automation LTEE, Canada) which measure the particle temperature (T) and velocity (V). Usually the diagnostics is carried out before the actual spraying on the sample. The spraying parameter is set and the powder is fed into the plume. Usually a much lower federate is used while carrying out particle diagnostics. The torch is then moved to the diagnostics position to measure the particles' temperature and velocity. The DPV2000 measures up to 5000 particle counts. Though the T and V data obtained is only an average value; it still gives an estimate on the particle conditions for a given processing condition. The AccuraSpray works by measuring the particles T &V as an ensemble. This sensor is used to carry out the injection optimization as it gives an estimate of the position of the particles in the plume. Post particle diagnostics, the torch is moved to its home position and the powder feeding is turned off. The substrate is then preheated. As a practice around 3 to 4 preheats passes are carried out. After the end of the last preheat pass, the torch is again moved back to its home position. The powder feeding is started and the torch is programmed to spray the desired number of passes on the mounted substrate.

3.4. Specimen preparation

The coatings were deposited on Al beams (Al 6061) of 9"x1" dimension. The dimension was chosen as per the requirement of our bi-layer curvature measurement. The 9:1 ratio was decided to avoid any out-of-plane stresses in the coating. In order to ensure better adhesion between the coating and the substrate, the surface roughness of the substrate is increased by the process of grit blasting. During grit blasting

compressive stresses develop in the beam due to peening, and beam tends to bend towards the un grit blasted side. Hence in order to balance the stresses, both sides of the beam are grit blasted. The curvature of the beam post grit blasting is measured. The beam is cleaned with alcohol prior to grit blasting. The samples are then grit blasted at 40psi. Care needs to be taken while doing this so that the beam does not get bent due to the stresses on it during the grit blasting. A uniform and controlled grit blasting is essential to get an even surface roughness. AlO_2 (grit size #24) particles were used during the grit blasting. Once grit blasted, the beam is once again cleaned with alcohol.

3.5. Thickness, weight and curvature measurements

The thickness, weight and curvature of the substrates are measured before and after coating deposition. This enables the computation of coating thickness, weight and hence the density. The density is calculated from the weight and volume of the coating using the formula shown below[12][15].

$$\rho = \frac{w}{t \times w \times l}$$

In spite of grit blasting both the sides of the substrate, there would be some residual curvature present in the coating after grit blasting. Hence it is essential to measure this value of curvature prior to the coating deposition. After the spraying once the coating cools down, the residual curvature of the beam is measured and its difference from the curvature after the grit blasting is used as the actual curvature change due to the coating deposition. The curvature measurement is carried out using a dial depth micrometer (Compac Geneve). The micrometer measures the deflection at three (two

ends and center) on the beam and those are fitted to the equation of a circle to obtain the curvature.

4. Evaluation of Mechanical Properties of Coatings using Bi-layer Curvature Method

The developments of stresses in coatings play an important role in governing the coatings' microstructures and thereby on their properties and performance. Understanding the cause and effect behind this is of utmost importance. In plasma sprayed coatings one of the main reasons for stresses to be generated is due to the quenching of the particles. The cooling of the particles on being deposited and the rapid solidification which follows cause these stresses. Once the entire layer of coating has been formed, the cool down phase starts. During this, the coating undergoes rapid cooling within the booth environment. The thermal expansion mismatch between the coating and the substrate induces a strain misfit between the two. As a result thermal stresses are generated within the coating. A detailed explanation of the various stages during the spraying process and the stresses associated with each stage are given in the following sections.

4.1. Stress evolution during spraying

During the process of spraying, the curvature measurements on the beam are measured using the ICP (In-situ Coating Property) sensor developed at CTSR. This consists of a fixture on which the beam is mounted and sprayed upon. Two contact thermocouples on either end of the fixture measures the substrate temperature during

the process of spraying[30-32]. Three lasers each separated by a distance of 74mm shoot on the substrate. The bending of the beam while spraying is measured by the laser displacement and then fitted to the equation of a circle.

The data generated by the ICP sensor post spraying provides valuable information on the real time stress evolution. The first section of the ICP data would correspond to the preheating of the substrate prior to spraying. This does not result in major curvature changes. After this section there is a drop in the temperature and a break in the data. This corresponds to the time the torch takes to return to its home position and to start the powder feeding. From there on each crest and trough in the ICP data corresponds to a pass during spraying. This continues till the desired number of passes. There is a significant change in the curvature from the end of preheating to the end of the first pass. This is the stress generated on the beam due to the impingement of the particles. The change in curvature between in each pass is not very significant and can be assumed to be almost constant. The slope of this line is the evolving stress in the coating. Positive value of evolving stress indicates that the stress generated during this phase is due to the rapid quenching of the splats after deposition[31]. At the end of the spraying process the coating would be in a state of tension. The rapid cool down of the beam then begins as indicated by the drastic drop in temperature in the ICP data. During this phase the CTE mismatch between the coating and the substrate governs the ultimate stress state in the coating. For a PS YSZ coating on an aluminum substrate, the CTE of the substrate is more than that of the coating. This leaves the coating in a compressive stress state finally.

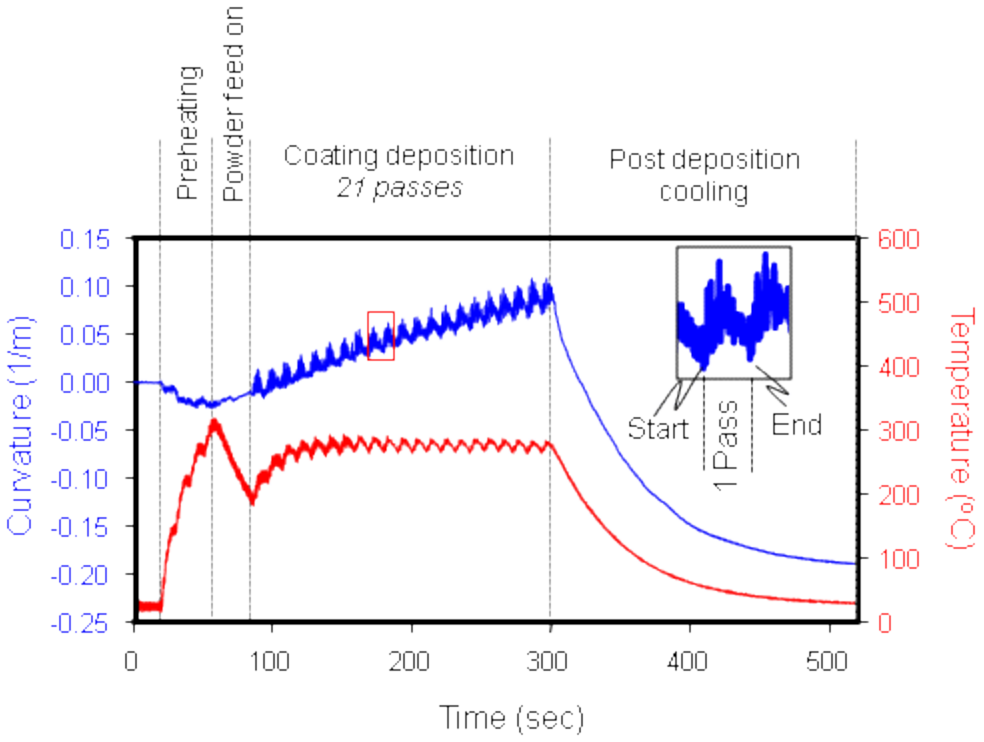

Figure 4-1: Data acquired from the In Situ Coating Property sensor depicting the evolution of stresses during spraying. The change in the temperatute profile during the preheating and the actual spray passes is also shown[12]

4.2. Elastic modulus calculation

The elastic modulus of the coating governs the residual stress present in the coating. Some of the ways of measuring coating modulus are by tensile testing, micro indentation, compressive testing and flexural testing. Our system consists of a substrate and a coating. We thus utilize the bi layer theory for the computation of elastic modulus of the coating. For this, we measure the curvature change in the system upon thermal loading. The expression for such as system is as follows[30, 33].

$$\Delta k = \left(\frac{6E_c^{'}E_s^{'}t_c t_s (t_c + t_s)}{E_c^{'}t_c^4 + E_s^{'}t_s^4 + E_c^{'}E_s^{'}\left(6t_c^2 t_s^2 + 4t_c^3 t_s + 4t_c t_s^3\right)} \Delta\alpha \right) \Delta T; \quad \text{..... Eq. (4.1)}$$

$$E_c^{'} = \frac{E_c}{(1-\nu_c)} \;\&\; E_s^{'} = \frac{E_s}{(1-\nu_s)}$$

Here Δk is the change in curvature and $\Delta\alpha$ is the difference in the coefficient of thermal expansion in the between the coating and the substrate.

The technique of measuring curvature of specimens during their thermal cycling has been very well established. It has been used extensively to compute the mechanical properties of thin films. The basic principle is that when a bi-layer system is subjected to thermal loading, it undergoes a strain mismatch. The stress induced as a result depends on the properties of the film and the unbalanced forces result in the curvature change in the system. For thin films the through thickness stress can be assumed to be uniform and hence, the general Stoney Formula can be used.

4.3. Substrate Curvature Temperature Measurement

In order to understand the anelastic behavior in plasma sprayed ceramic coatings, a novel substrate curvature temperature or Bi Layer Curvature Temperature measurement (BCT) was introduced[34]. The basic mechanism involves computing the curvature of a coated beam and deriving the anelastic properties base on various equations. Upon thermal cycling, the beam gets heated. The coating (YSZ) and substrate (Al) have a different CTE. The Al substrate with a CTE of $24 \times 10^{-6}/^{o}C^{-1}$ tends to expand more than the ceramic YSZ with a CTE of around $9 \times 10^{-6}/^{o}C$. As a result there is a strain misfit within the system as a whole. In order to accommodate this strain misfit the beam bends. As the beam bends, the displacements of the lasers change. From the difference

of the initial displacement to the final displacement, the extent of curvature change in the beam can be computed. The experimental setup consists of a furnace which heats up the sample. Three lasers are pointed on the beam at three different points along the length of the beam. Before starting the BCT measurement the beam's thickness and residual curvature are measured. The coated beam is then mounted in such a way that the coating faces the lasers. A K type thermocouple is used to measure the temperature of the beam. It is attached on the uncoated side of the beam. Care must be taken that there is no room between the thermocouple and the substrate at their point of contact. Air tends to flow through the gap and induces localized cooling of the substrate right next to the thermocouple and gives erroneous values for temperature. Another factor which needs to be taken care of is the accumulation of moisture as well as dust on the laser windows. Such foreign media on the laser window would decrease the lasers' intensity. Hence it is advisable to clean the windows periodically

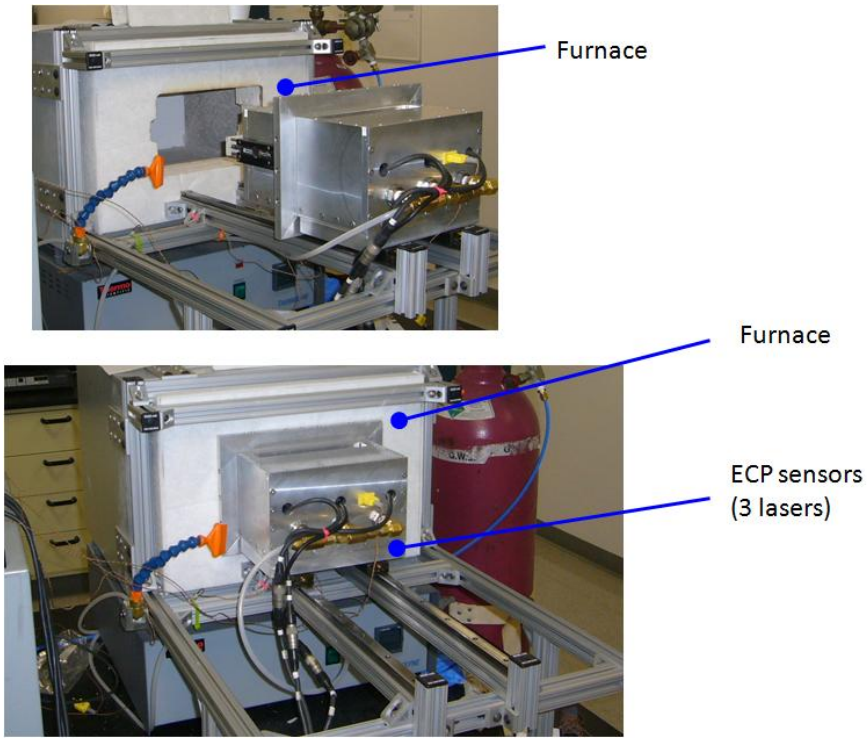

Figure 4-2: Experimental setup of the Bi-layer Curvature Measurement Technique. The system consists of a furnace and a sensor head. The specimen is mounted on the sensor head with three lasers shooting along its length. The sensor head is moved into the furnace during the testing

The BCT box consists of channels which circulate air through them. This is to ensure that the lasers do not get damaged at high temperatures. The lasers can function up to a maximum temperature of 40°C. The data is collected using CTSR's in-house software Kurvaware. In order to cool the furnace an air blower and an auxiliary fan are provided. Initial trials were carried out with thermocouples along the length of the beam .The temperature variation along the length of the beam as well as the two faces namely the bare one and the coated have been found to be very negligible. Hence using a single thermocouple anywhere near the center of the beam is good enough to measure the temperature during the thermal cycling. A water chiller has also been installed to facilitate the thermally cycling up to higher temperatures of around 500-600°C. The

water circulates through the channels provided inside the BCT box. However at such high temperatures the regular K type sticky thermocouple cannot be used as it tends to get burnt. Hence under such circumstances a pyrometer needs to be appended to the experimental setup. Prior to using the pyrometer one needs to calibrate it. In order to do this we take a test sample and attach a regular sticky thermocouple to it. The pyrometer is connected to the experimental setup. The sample is then cycled to a temperature of around 400^{o}C. The data is acquired and the temperature readings corresponding to the thermocouple as well as the pyrometer are plotted. Beyond a temperature of 300^{o}C, the sticky thermocouple would have got burnt and would have most likely detached itself from the substrate. The slopes of both the graphs are computed. The value of the calibration factor is then computed and incorporated into the data obtained from the pyrometer. Once the pyrometer has been calibrated, it can be used during high temperature cycling of the BCT experiment.

Hence to achieve ultimate reliability on the data, there was a need to cycle the beam under a controlled environment. It was this requirement which initiated the induction of the present generation BCT measurement equipment. This was a furnace into which the beam would slide in. The heating cycle to around 250^{o}C substrate temperature took 30 minutes. At the end of the heating, an auxiliary fan would be turned on to uniformly cool down the sample. The cooling cycle takes around 2hours. Once the temperature of the beam comes down to around 40^{o}C the beam is taken out of the furnace. At this point the beam would have undergone a very uniform cooling cycle and hence there would be no drastic change in the curvature of the beam. Hence a very smooth heating and cooling was obtained. If the beam is taken out of the furnace at higher temperatures, the system cools down faster as is it is then being subjected to atmospheric conditions. However there is a very evident kink in the cooling cycle. This could affect the

computation of the hysteresis degree (*HD*)[35]. Though the cooling data is smooth it is still unclear as to how much effect the faster cooling with the auxiliary fan has on the overall anelasticity of the coating.

A typical curvature temperature plot has been shown in the figure below .As one can see, there is heating cycle and a cooling .The temperature range over which the thermal cycling is carried out is T_m and T_{max}. The temperature T_{tr} corresponds to the transition temperature. Till the transition temperature the system behaves linearly and beyond that the nonlinearity in the system starts. One observes that for the heating and the cooling the coating follows a different path upon loading and unloading.

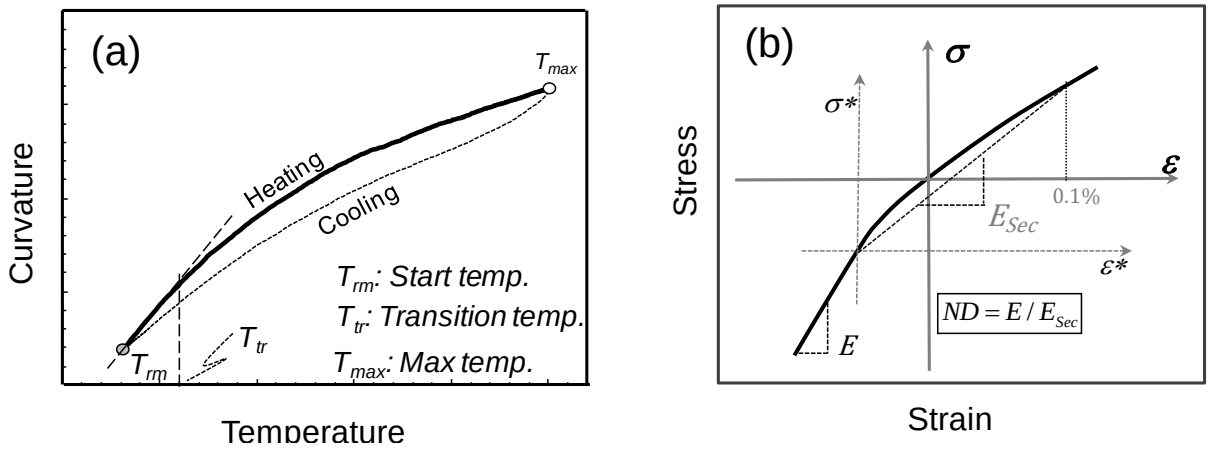

Figure 4-3: A typical curvature -temperature plot showing the various regimes the system goes through. Also shown is stress-strain graph depicting the nonlinear beahvior of the coating

4.4. Calculation of anelastic parameters using non-linear model

In order to quantify the nonlinear properties of plasma sprayed YSZ coatings a uniaxial stress –strain model was developed by Nakamura et al. To use the model one needs to provide some data as the input. These are coating and substrate thickness, residual curvature of the beam, the temperature range across which the analysis is to be executed and the transition temperature. The transition temperature is chosen manually by drawing a line along the curvature –temperature plot and determining the point beyond which the coating exhibits nonlinearity. The model converts the curvature – temperature data to stress-strain[26].

$$\varepsilon = \begin{cases} \dfrac{\sigma}{E} - \dfrac{\left|\sigma_T\right|^n}{E\sigma_N^{n-1}} & \text{for} \quad \sigma < \sigma_T \\ \dfrac{\sigma}{E} + \dfrac{(\sigma-\sigma_T)^n - \left|\sigma_T\right|^n}{E\sigma_N^{n-1}} & \text{for} \quad \sigma \geq \sigma_T \end{cases} \qquad \text{..... Eq. (4.2)}$$

As per this model the secant elastic modulus of the coating is computed at 0.1% strain. This value of strain has been chosen based on a number previous trials and experiments carried out on PS YSZ coatings. It has been observed that most of these coatings would pass through this regime of strain. In the above expression the terms n and σ_N correspond to the power law exponent and the reference stress, respectively. The term σ_T is the transition stress. This is the value of stress at the transition temperature of the coating when the coating goes from linear to the nonlinear regime. Ideally all the cracks should be opened above the transition stress state because beyond this their opening causes the nonlinearity in the system. However the cracks are not oriented in a particular direction for them to open and close at the same time. Hence it is possible that even above this point certain cracks are closed. This also explains why the

nonlinearity is not a sharp change and is rather a smooth transition. The transition stress is mostly negative in the case of YSZ on Al. The modulus computed here is the room temperature elastic modulus of the coating and not at zero stress state. There are certain important criteria which the model considers.

It is assumed that initially when the coating is under compression most of the cracks and pores are closed[16][26)61]. Hence the response is expected to be linear. Secondly the asymmetric nature of the stress strain relation is considered under both compression and tension. Finally it is assumed that the transition from linear to nonlinear regime does not occur at zero stress state. The nonlinear model though quite robust, comes with its own set of shortcomings.

Firstly the model can only be used for a coating which exhibits a linear behavior followed by a nonlinear behavior. Coatings which display any other behavior would not be compatible with this model. It is essential that post spraying at the room temperature condition the coating must be under a compressive state. Thirdly the curvature corresponding to the transition temperature should be negative. During the thermal cycling the specimen should experience the state of zero curvature state between the transition temperature and the maximum temperature.

From this nonlinear model one of the anelastic parameters namely the nonlinear degree is extracted[27]. It is defined as the ratio of the tangent elastic modulus to the secant elastic modulus[27].

$$ND = \left(\frac{E}{E_{\sec}} \right) \qquad \text{…….. Eq. (4.3)}$$

In the above equation E is the value of elastic modulus at room temperature. The secant modulus is chosen as the slope between the transitional point and the point at additional 0.1% strain .A nonlinear value of one indicates a linear elastic coating and the higher values of ND correspond to coatings with greater nonlinearity. The two parameters ND and E are obtained once the analysis is carried out. These two are computed based on the heating section of the curve. In order to compute the degree of hysteresis HD, one needs the entire heating and cooling loop. It is computed as the ratio enclosed by the stress strain curve to the rectangular region given by $\Delta\varepsilon \times \Delta\sigma$. These three anelastic parameters are used in unison to characterize various plasma sprayed coatings.

4.5. Sensitivity of the Anelastic Parameters

The sensitivity of the BCT measurement technique was evaluated by varying the processing conditions of the coatings. Three coatings low, medium and high energy were sprayed on aluminum substrates. The conditions were chosen to introduce significant porosity level differences in coatings. Thermal cycling was carried out on them and the nonlinear parameters were evaluated.

The high energy condition resulted in a denser coating. As a result the stiffness was of this was observed to be the highest. The inter splat cohesion in this case would have been good and this would mean that coating had relatively less amount of interfaces and defects. Upon thermal cycling the beam goes from compressive state to tensile state. The lesser defect density resulted in a lack of significant nonlinear behavior. The hysteresis was also found to be less due to the lack of interfacial effects. On the other hand the coating sprayed with the lowest energy condition would have been more

porous in nature. Since the plasma energy is lower it does not melt the particle sufficiently. As a result the deposited coating consists of unmolten particles successively deposited one over the other. Such a deposition process would result numerous defects, cracks and interfaces in the coating architecture. Upon thermal loading, these crack interfaces slide over each other thereby lending the coating its nonlinearity. There is a lot of interfacial friction when these surfaces slide. This results in higher value of *HD* for such a coating as shown in Figure 4-4. The coating sprayed with a medium energy plasma condition should thereby ideally lie in a region between the aforementioned coatings on a process map. The same is what was observed after the nonlinear analysis. Figure 4-4 clearly elucidates the results.

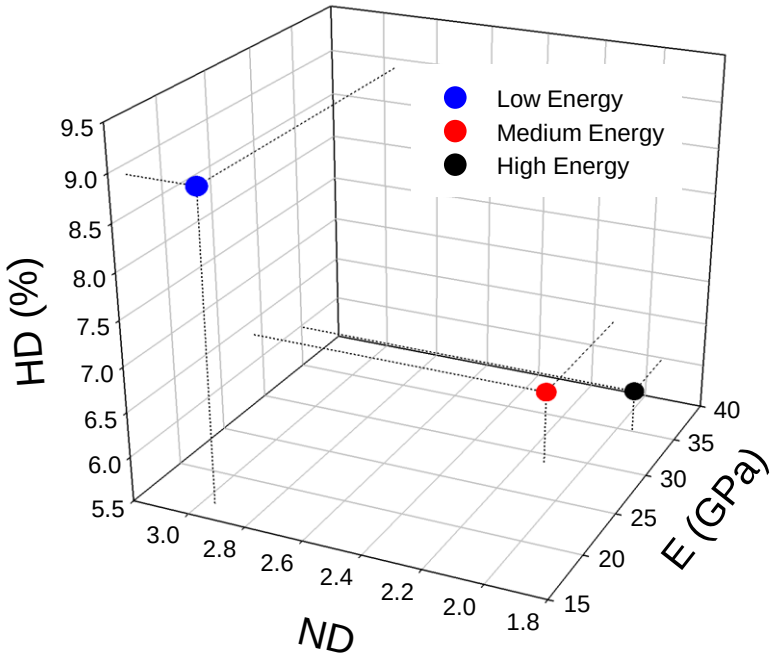

Figure 4-4: A plot showing the sensitivity of the anelastic parameters to the variations in processing conditions. The results show three coatings sprayed at three different plasma energy conditions

Having established the sensitivity of the anelastic parameters to three extreme processing conditions, one feels the need to gain confidence in the data obtained. This could be made possible by a systematic error analysis of the system. The repeatability of the anelastic computations is another aspect which needs to be understood. Do the same coatings generate the same values of anelasticity upon repeated trials or are there any errors introduced? These and more are the focus areas of the next chapter in this thesis.

5. Repeatability and Sensitivity Analysis of Anelastic Parameters

Similar to any other measurement technique the quantification of anelastic parameters from BCT measurements can contain some degree of errors. These errors could be an artifact of the instrument or measurement technique. For instance, in the case of BCT measurement on one hand an improper placement of thermocouple can introduce errors in temperature measurement; on the other hand the varying temperatures over different seasons of the year can affect the heating and cooling rate for the thermal cycle. Similarly, computation of anelastic parameters can be erroneous if the required input parameters such as thickness and residual curvature numbers are off by some percentage. Therefore, the ultimate impact of these errors on the anelastic parameters of the coating being reported needs to be known. The sensitivity of the anelastic parameters on such errors has also been understood. Though it might appear

quite trivial, their implications on the final data could have a telling effect. This chapter will present results from an analytical study conducted to address both experimental as well as computational error. Later, the fidelity of anelastic parameters obtained from analysis on multiple coatings sprayed at constant parameters will be reported.

5.1. Experimental Repeatability

As in any experiment, an estimate of the error is important to gain confidence in the data. This study is carried out to investigate the errors associated with experimental procedure only. BCT thermal cycling of three samples was done continuously for 10 cycles. The non-linear analysis was then carried out treating each of those cycles independently. The same procedure was carried out for 3 different process conditions. The plasma energy was kept at high, medium and low conditions for each of the coatings. The same thermocouple was used for all the 10 cycles of a specimen. For the same sample when cycled multiple times, the curvature –temperature response should ideally be the same for a perfect system. However, with the current setup the strain rates cannot be controlled and hence minor variations as an artifact of the furnace could possibly occur. Additionally, day-to-day temperature variation can also introduce some variability in measurement. For each of the 10 cycles, the temperature range over which the analysis was carried was kept constant. The other input parameters for the nonlinear program such as the transition temperature, coating and substrate thickness were also maintained constant.

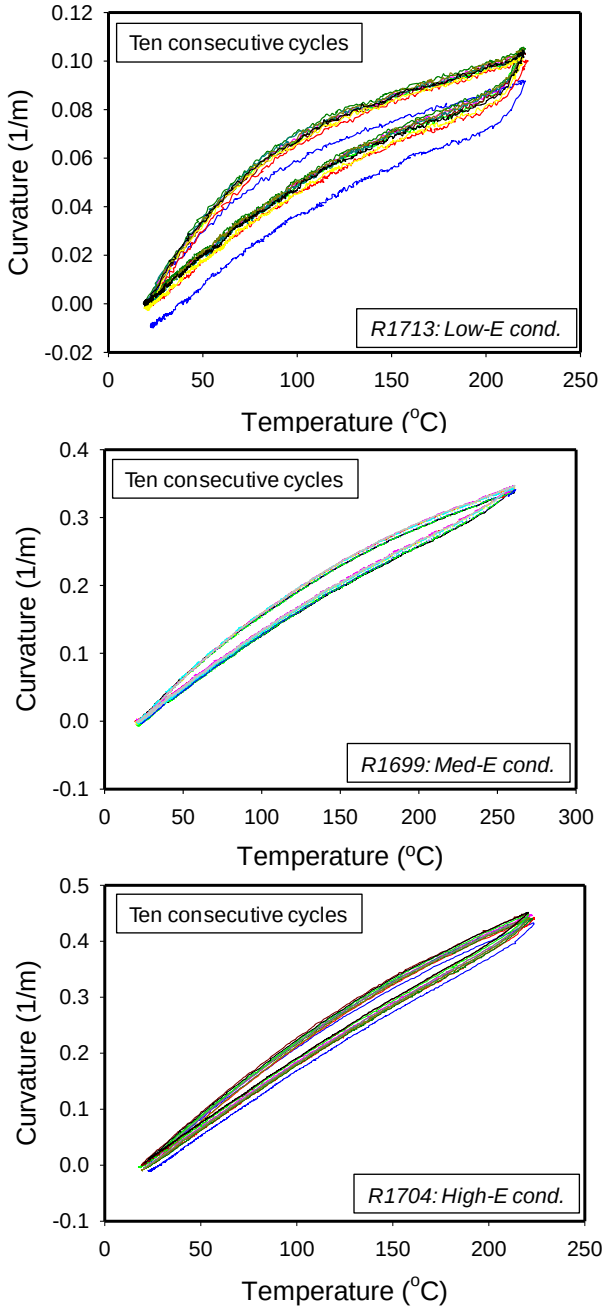

Figure 5-1: The curvature -temperature response of the three coatings obtained from multiple BCT measurements. The coatings were sprayed at different plasma energy to introduce different levels of porosity. The first cycle (in blue) is invariably different in all the three coatings. By visual inspection one can notice that the Low-E coating exhibits larger variability in curvature-temperature response as compared to the other two

5.2. Sensitivity Analysis

Apart from the experimental repeatability, chances of having some variability induced from the various input parameters for quantification of anelastic parameters may arise. For instance the measurement of coating and substrate thicknesses by two individuals can lead to some discrepancy in the data collected. Such differences may affect the quantified parameters significantly. Therefore, another study was conducted to understand the variation in the convergence of the non-linear program for the same sample on multiple occasions. The sensitivity of the non-linear parameters to variations in substrate and coating thicknesses as well as transition temperature was evaluated. For a single coating, the nonlinear analysis was carried out with ten different values of input parameters. For each case, one of the parameter was changed systematically without changing the other two parameters. The output parameters were then plotted with respect to the modified input parameters.

Based on previously reported data, in order to see a significant change in curvature, the thickness of the coating needs to be at least more than 300μm[12] [15]. Therefore to avoid any error induced due to insufficient curvature change, the coating was chosen with an approximate thickness of 300μm. The substrate thickness for this case was set to its standard value at 2.24mm. Another parameter considered here was the transition temperature which corresponds to the linear to non-linear transition stage. Due to the manner in which it is determined it can vary from person to person, as the transition occurs smoothly over a small region of temperature change rather than a sharp point in the curvature-temperature plot. Since the sliding of the cracks governs the transition temperature its exact point of initiation is tough to pick. Hence though the non linear behavior is quite evident, its exact initiation is extremely subjective.

5.3. Design of Experiments

The first experiment was designed to examine experimental error introduced by the BCT instrument and measurement procedure. Three different batches of YSZ coatings on aluminum substrate were deposited. All the coatings were sprayed at 150mm spray distance and the processing conditions were changed for the three coatings. The corresponding plasma parameters are listed in Table 5-1. The parameters were chosen to produce coatings with significantly different defect architectures. Figure 5-2 shows the SEM micrographs of the coatings processed using the three parameters. This experiment was specifically designed to investigate the effect of porosity on the repeatability of coating performance.

Run #	Specimen ID	Ar flow rate (Lpm)	H_2 flow rate (Lpm)	Amperage (A)	Voltage (V)	Plasma Power (kW)	Coating Thick. (mm)
R1713	Low E	35.2	2.6	450	48	22	0.3013
R1698	Med E	47.5	6	550	60	34	0.3852
R1705	High E	60.1	11.2	650	72	47	0.4472

Table 5-1: The various process parameters during the plasma spraying of the three coatings

To keep other possible errors restricted, a new thermocouple was used for each specimen, and was kept attached for all 10 cycles Due to long thermal cycle time, on a given day only two sets of heating and cooling cycles can be performed. This exposes the specimen to ambient moisture condition overnight at the end of the day. Therefore to negate the effect of moisture on our analysis the beam was also preheated everyday to around 100°C before the actual thermal cycling. After the initial preheating of the

furnace the beam was cycled in the usual manner. Each of the coatings was thermally cycled ten times and the nonlinear analysis was carried out on the data obtained from each cycle. The same process was followed for all three coatings.

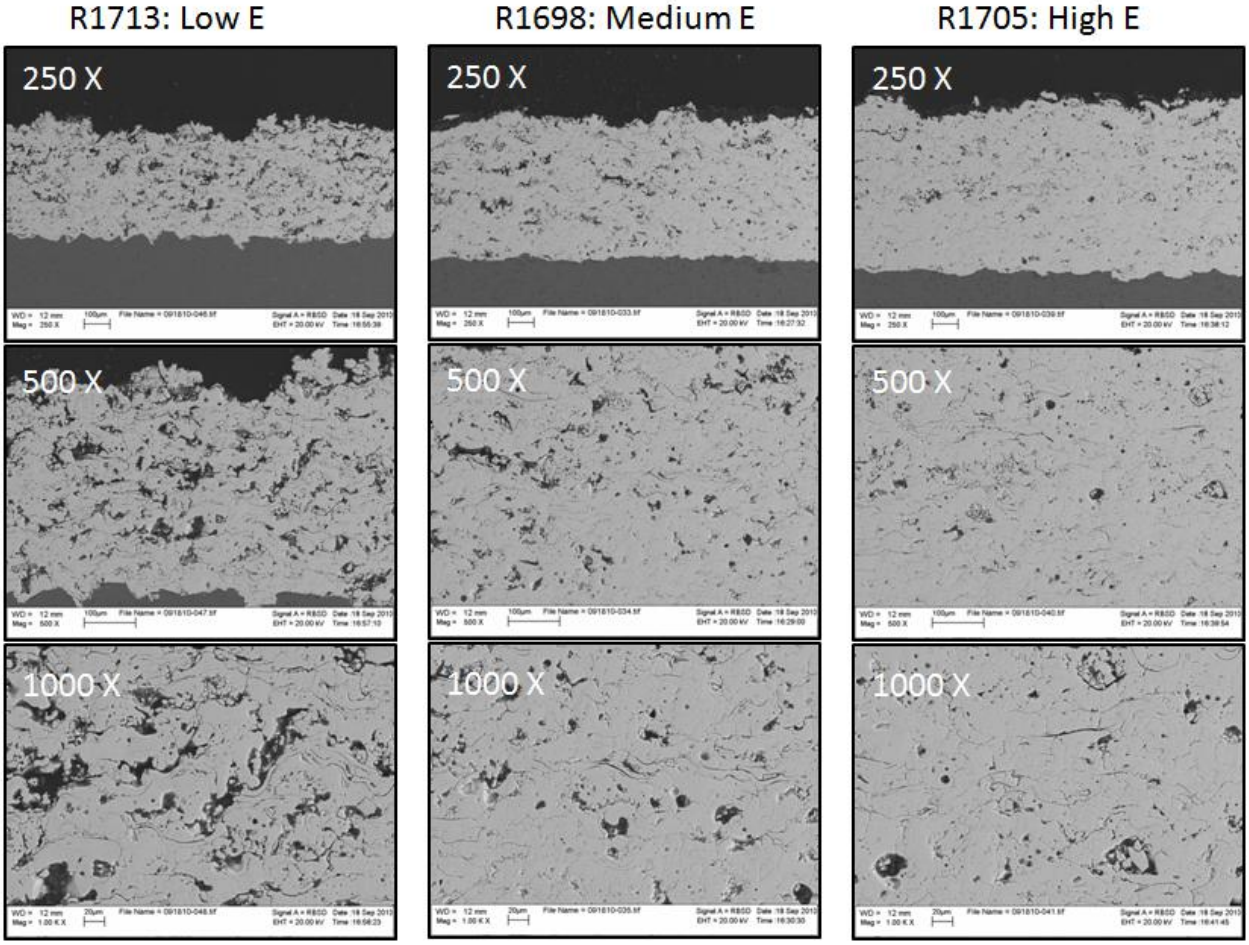

Figure 5-2: SEM images elucidating marked differences in the porosity levels of the three coatings sprayed at three different plasma energy conditions. Due to the variations in the particles' melting it can be observed that while the low energy plasma condition produced an extremely porous coating the higher energy conditions produced very dense coatings

5.4. Results and Discussion

Among the three samples, the error varied depending on the extent of curvature change undergone during the BCT measurement. The data of first cycle is not included for analysis as this particular cycle is a phase during which the system adjusts itself Therefore, the data for nine consecutive cycles was used to understand the variability.

The number of coating passes were kept constant, however that meant that the thickness as well as thickness per pass varied significantly among the coatings (table 5.1). This could be attributed to the different deposition efficiency of the process. The better melting of the particles in the plume ensures that at the time of contact with the substrate the particles are in a sufficiently molten state. On the other hand, if the injected particles were to remain unmolten the adhesion with substrate and the cohesion between particles would be suppressed. This would result in lower deposition efficiencies during the coating deposition[24] [39]. The plasma enthalpy was changed by tuning the process parameters (Table 5-1), which produced particles with different melting states. With variations in the melting index of the particles the extent of porosity in the deposited coatings change as illustrated in Figure 5-2.

As mentioned earlier, the low energy condition generated a thinner coating when compared to the medium and high energy conditions (Figure 5-2). This will influence the response of the coatings when subjected to thermal loading in the BCT measurement technique. Since the BCT measurement relies strongly on the extent of curvature change the system undergoes, it is important to understand the phenomenon behind it .The strain generated between coating and substrate due to thermal expansion mismatch, causes the coating-substrate system to undergo a curvature change. If the strain at the interface is higher the system would undergo more curvature change

during the thermal cycling in order to accommodate them. Under lower strain conditions at the coating-substrate interface the curvature change produced upon thermal cycling would be relatively less. Therefore, even two coatings with similar elastic modulus but different thickness will lead to difference curvature change for a given temperature change. In short, it's the stiffness of coating which governs the curvature change primarily. A higher curvature change signifies that the low signal to noise ratio and that a clearer and more reliable data is obtained. In contrast, with thinner coatings the signal to noise ratio would be higher which will introduce large amount of noise in the measurement and may significant induce errors in the non linear analysis.

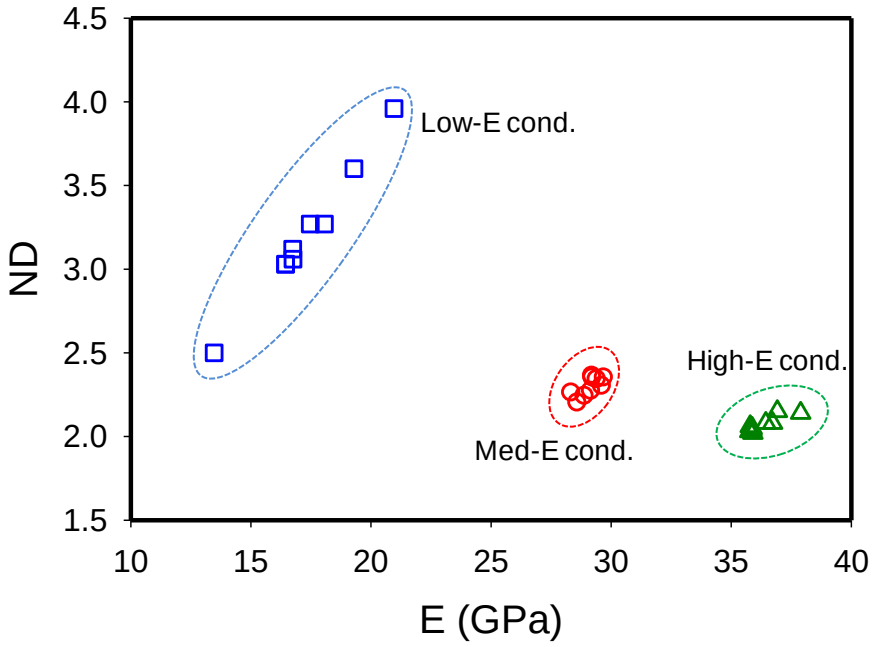

Figure 5-3: The variations in the computed values of *ND* and *E* values upon consecutive thermal cycling followed by BCT measurement. Coatings sprayed at lower plasma energy conditions show more variations in the computed values due to presence of defects in them. Coatings with relatively lesser defect density exhibited better repeatability in the computed values

The nonlinear analysis carried out on each cycle revealed certain startling results. The plot of *ND* vs. *E* (Figure 5-3) indicates that the nonlinearity of the coatings vary systematically. The elastic modulus of the three coatings can easily be explained by the overall defect density. The lower defect density coating (High-E) exhibited higher elastic modulus followed by Med-E and Low-E having medium and high degree of porosity correspondingly. The coating sprayed at lower plasma energy condition exhibited higher nonlinearity which could be attributed to the higher defect density in it. The medium and high energy plasma condition produced coatings with systematically lower nonlinearity, which could be explained based on the densely packed nature of these coatings. Between them, the medium and high energy conditions did not show drastic difference in the nonlinearity. This can be attributed to the adequate thickness as well as relatively comparable porosity level as substantiated by the SEM images (Figure 5-3).These observations are supported by their raw curvature-temperature responses shown in Figure 5-1, and the results obtained from the nonlinear analysis as well as the SEM images of these coatings seemed to concord on the nonlinearity front.

Another interesting observation is the distribution of the data upon repeating the BCT measurement. The lower energy condition generated numerous pore and defects. As a result the overall thickness of the coating could have decreased resulting in a very low signal to noise ration during the BCT measurement. Thus when the nonlinear model attempts to converge the raw curvature –temperature data, there could have been variations in the data points acquired by the numerical model. The repeatability study on the medium and high plasma energy conditions yielded results with a very tighter distribution of the nonlinear parameters with higher degree of convergence as compared to low energy condition one.This indicates that the densely packed coatings

are able to generate more consistent results due to the relatively lesser defect density as well as the lower mobility of the defect interfaces. The standard deviation (SD) in the values of *ND* and *E* represent the quantified variability associated with the measurements (Figure 5-4). While the coating sprayed at the low energy condition showed the highest SD value of 0.40 and 2.08 GPa for nonlinear degree and elastic modulus respectively, the medium and high energy conditions show much lower values. This further reaffirms our previously stated hypothesis that the presence of higher defect density not only changes the nonlinear parameters but also affects the repeatability of the BCT measurement. Thus, though the BCT measurement is quite reliable, the computational error could be of a relatively higher degree for thinner coatings than for thicker coatings. This study provides some useful information regarding interpretation of anelastic parameters. Especially, when comparing the coatings sprayed at constant parameters, one should keep in mind the higher variability with high porosity coating. Additionally, it is important to conduct the BCT measurement with adequate coating thickness capable of providing sufficient curvature change during thermal cycling.

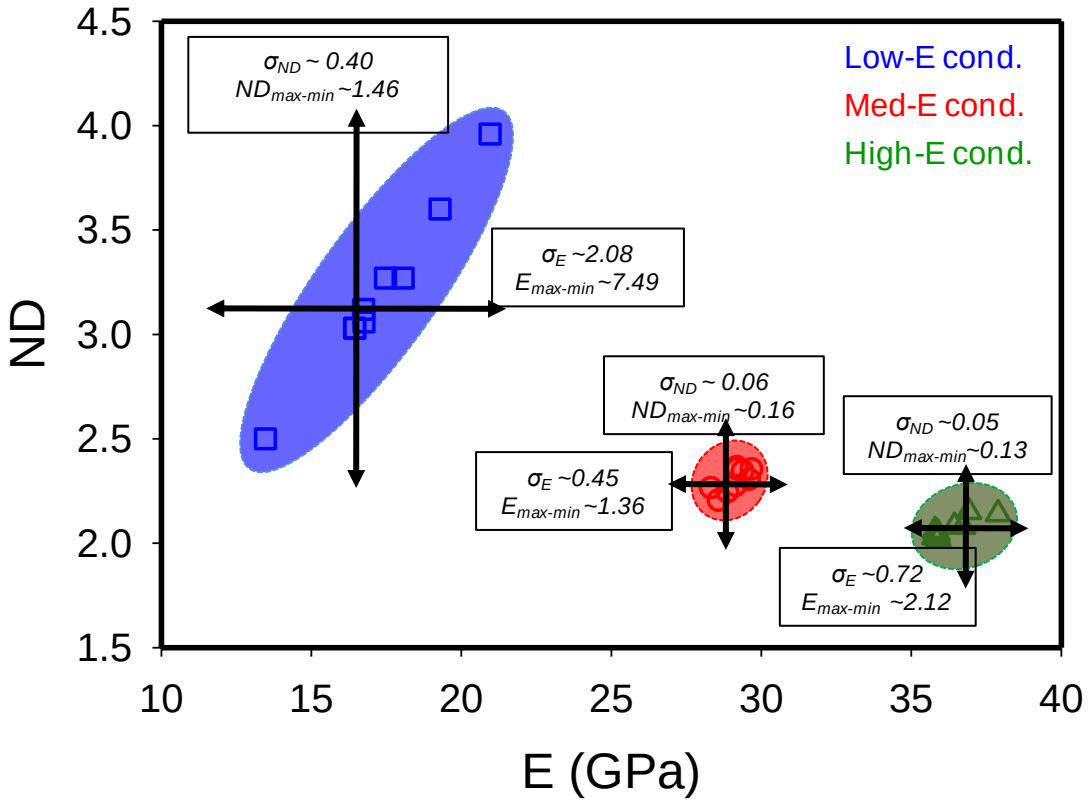

Figure 5-4: Standard deviation and maximum-to-minimum range of the analyzed nonlinear parameters for the three coatings. Maximum standard deviation in *ND* as well as *E* in the low energy condition could be attributed to the larger defect density

Having understood the repeatability of the nonlinear analysis to experimental error, the next step taken was to estimate the influence of errors associated with the input parameters on the computation. This could be in the form of computing coating and substrate thickness. As mentioned earlier, in order to carry out the nonlinear analysis there are certain input parameters one needs to optimize to obtain the maximum possible convergence for a given set of data. These are the reference stress σ_N and the power law exponent n as shown in following equation used to generate stress-strain relationship from the BCT measurements[16][26].

The range of the reference stress and the power law exponent need to be adjusted constantly in order to achieve the highest degree of convergence. Apart from this the mathematical model needs the curvature temperature data acquired from the BCT measurement, thicknesses of substrate and coating, and the residual curvature imparted to the system due to spraying. Additionally one also needs to specify the range of temperature over which the nonlinear analysis should be carried out .Usually a large window is provided to enable the program to converge effectively , however if for some reason the data along a particular regime appears noisy , then the input ranges are adjusted suitably. In the input file for the program one also needs to specify the transition temperature for the given coating system. This is the region beyond which the coating begins to exhibit nonlinear behavior and hence is coating specific. Among all the above mentioned input parameters needed to carry out the nonlinear analysis it is quite clear that there could be three major sources of error: the thickness of the coating and substrate and the transition temperature. These three can be considered more prone to introducing error in the analysis as they are quite subjective and can vary from one user to another. Hence in this last part of this chapter computational errors have been deliberately introduced to quantify the magnitude and impact that such variability could bring to the final results obtained from the nonlinear analysis.

We start off by introducing systematic errors in the thickness of the coating and substrate and carry out the nonlinear analysis treating each of these as a separate condition. The curvature-temperature data obtained from thermal cycling of specimen number R-1698 (Med-E) sprayed at medium plasma energy condition was used The range of input parameters errors are chosen based on the experience gained on the analysis conducted over multitude of specimens. For the sake of clarity, instead of absolute values, only variations in the input parameters are shown in Figure 5-5 and

Figure 5-6. The "0" value on the horizontal axis corresponds to the actual measured value of that parameter for the given coating.

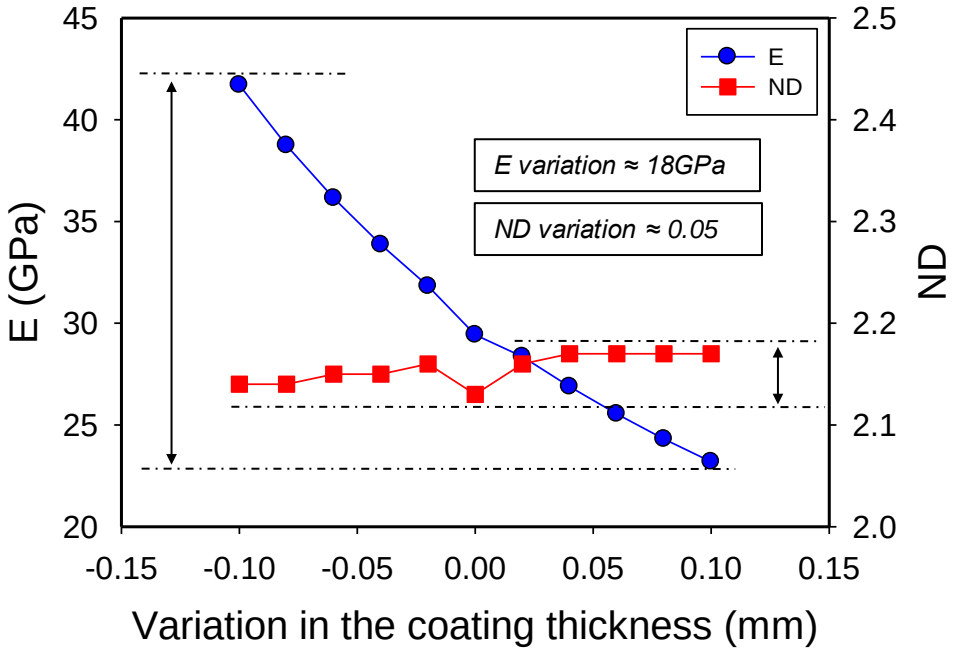

Figure 5-5: Plot indicating the extreme sensitivity of elastic modulus to the variations in coating thickness

Figure 5-5 shows the variation in output parameters due to error introduced in coating thickness. It was observed that with an increase/decrease in coating thickness the value of elastic modulus changed significantly. A difference of 18 GPa in the value of elastic modulus can bring the coating to a different regime of properties. This suggests that a lot of emphasis should be laid on the accurate measurements of simple but vital data in order to obtain accurate results of nonlinearity. Additionally, the linear trend of elastic modulus decrease with the increase in error towards higher coating thickness is noteworthy. The sensitivity of the nonlinear degree to errors in coating thickness was not very significant. A linear trend was obtained, however there is a

slight kink in the linear trend which still remains unclear and would need a more detailed investigation.

The introduction of errors in the substrate thickness again did not seem to influence the nonlinear degree, however difference in elastic modulus numbers are not negligible (Figure 5-6). . Hence during the execution of the nonlinear analysis to compute the anelasticity of coatings extra care needs to be given to the measurement of both coating and substrate thickness. One should be considering the possible error windows for each coating before interpreting the non-linear parameters.

Next we introduce changes in the transition temperature for the nonlinear analysis. Since the transition from linear to nonlinear regimes follows a smooth trend the selection of transition temperature appears to be very subjective. The introduction of systematic errors in its value provided results as shown in Figure 5-6.

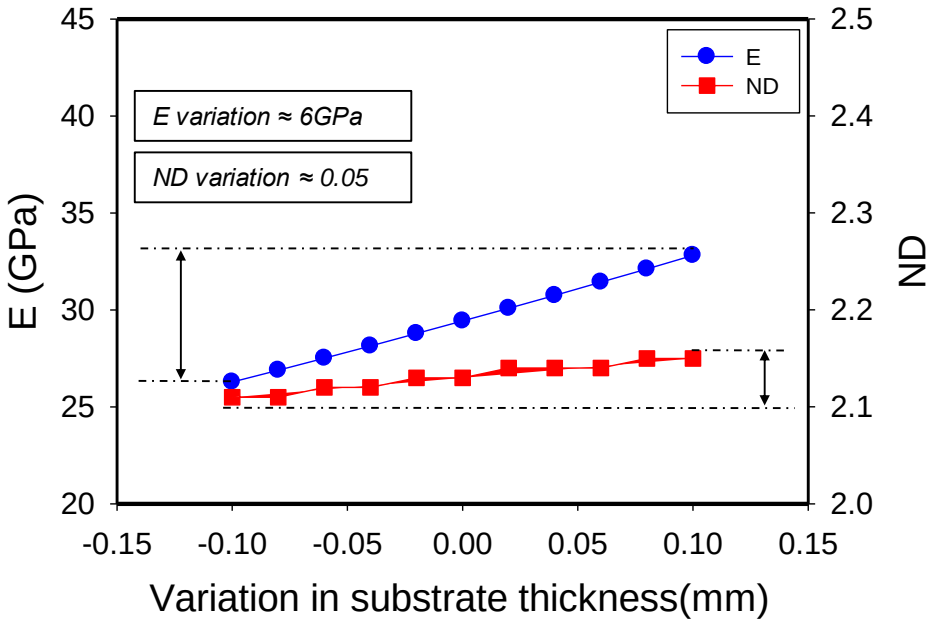

Figure 5-6: Plot indicating the sensitivity of elastic modulus and non linear degree to the variations in the substrate thickness

The algorithms designed to extract non-linear parameter do take care of slight variations in transition temperature selection, i.e. it averages the curvature for the values of transition temperatures ranging from ±2°C from the input numbers by user. However, some of the cases with less non-linear curvature-temperature plot, the error range can be much higher than ±2°C. Therefore, this study is also required to estimate the output errors (±5°C) due to input error in transition temperature.

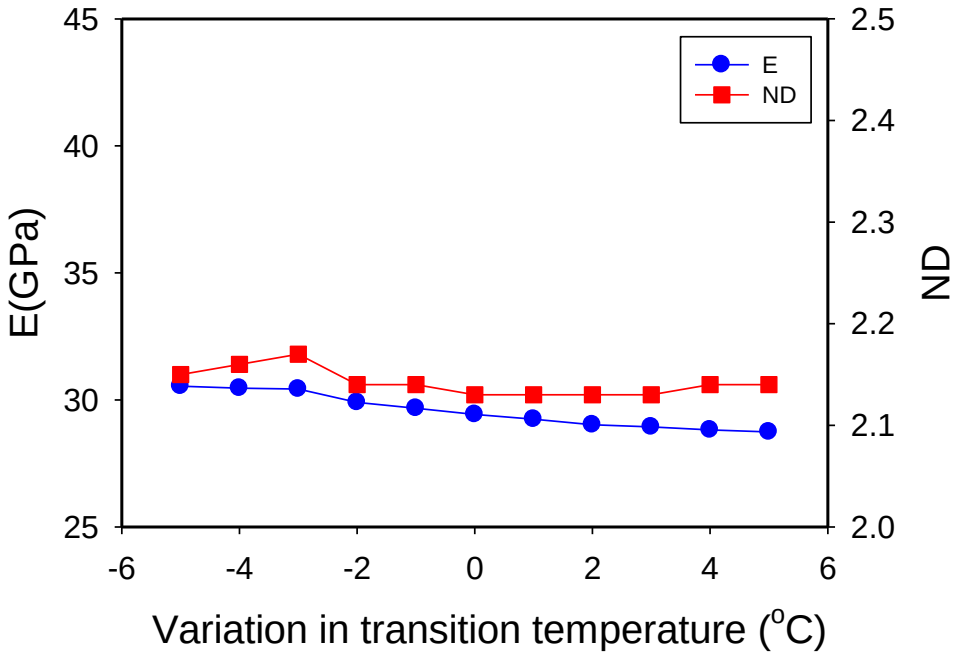

Figure 5-7: Plot indicating the sensitivity of Elastic modulus and nonlinear degree to the variations in the transition temperature

Figure 5-7 shows the change in non-linear parameters calculated with the errors in transition temperature measurements. The overall variation of the elastic modulus was around 3GPa, and that of non-linear degree was around 0.03. The non-linear degree variation is within the acceptable limit of quantified non-linear parameter, however the elastic modulus may be at the boundary conditions for its acceptable limits. . Based on

the results, it can be concluded that the numbers do not get influenced by slight errors in transition temperature, atleast for the case of errors upto ±5^{o}C . Though the degree of input parameters variation considered here may be beyond the practical situations, and the variations in output parameters are not relavent, nevertheless this study provides an insight into the error ranges associated with non-linear parameters. Important to note here is that the results discussed above are generated from the curvature-temperature response of a coating with adequate thickness and relatively higher density. They may vary from one coating to another coating due to different ranges experimental errors associated with the coatings.

Having established the basis for the possible sources of errors in this novel coating property sensor it is now possible to differentiate between artifacts and actual observations. The importance of measurements of coating thickness has been reiterated and results have been shown to further substantiate these claims. Apart from measuring the sensitivity of the BCT technique, its repeatability has also been investigated from a computational as well as an experimental perspective. Having gained sufficient confidence in the sensitivity of the BCT technique, we would be utilizing this in the forthcoming chapters to try and tailor the coatings' architecture by introducing changes in the process conditions Thus to conclude, the fidelity as well as the robustness of the BCT technique has been evaluated and this has provided better insights into decoupling the effects of intrinsic coating properties as well as artifacts in the form of errors.

6. Observation of Anelasticity Evolution with Incremental Strains

Having established sufficient basis for the anelastic parameters the next stage is to see if the anealsticity varies over different temperature regimes and hence to investigate the evolution of overall anelasticity with changing strain. It has been observed in the past that the first cycle of BCT measurement on a virgin specimen for a given temperature range is different from the successive ones. One preliminary reason for this unique behavior is explained by the fact that the coating adjusts its architecture for the strain range it is subjected to. A single specimen when subjected to different temperature regimes (beyond transition temperature) could show different extents of non linearity. Below the transition temperature the defects in the coating could be considered to be immobile due to compressive residual stresses. Hence for lower temperature cycles the measurements would show only linear behavior of the coating. While the temperature range is increased systematically, the curvature-temperature response starts exhibiting non-linear behavior correspondingly due to movement of the defects. Additionally the other component of anelasticity, the hysteresis, also changes with change in temperature range. The experimental design in this chapter will present the results revealing some interesting findings on the evolution of anelasticity with temperature changes. In addition, based on the conclusion from previous chapter regarding the porosity dependence on anelastic parameters, the study will be continued on the three coatings with different porosity levels. This investigation will provide an

insight on differences in anelasticity evolution for coatings with different degrees of anelasticity.

6.1. Design of Experiment

The same three coating R-1715 (low-E), R-1698 (med E) and R1705 (high-E) were used as discussed in Chapter 5. The specimens were cycled for a temperature range from room temperature to 100°C with increment of 50°C up to 300°C. For each temperature range, each specimen was cycled thrice, and, was cooled down inside the furnace to 40°C before starting the next cycle. Due to limitation with the current setup of BCT measurement, the exact control over the set point temperature was achieved after carrying out a couple of trial run without specimen. Additionally, due to the cooling requirement of BCT setup, there is usually a difference between the temperature of the furnace and the temperature of the beam being tested. Therefore, from the trial runs for different temperatures the required furnace temperature was estimated prior to the start of the actual experiment. Since it was not possible to carry out the entire experimental procedure in a single day , care was taken to ensure that the coating released any absorbed moisture overnight by preheating the specimen up to 100°C. Post preheating, the actual thermal cycling was carried out.

6.2. Results and Discussion

After cycling the samples to each temperature range the analysis was carried out to compute anelastic parameters and the values were plotted with respect to the set point temperature. All measurements obtained from the three cycles were analyzed Figure 6-1, 6-2 and 6-3 presents the results obtained from analysis for the three anelastic

parameters *E*, *ND* and *HD*. The values of *E* and *ND* values were obtained from the non-linear program (Chapter-4) while the *HD* degree was calculated by normalizing the hysteresis loop area with the total curvature and temperature change during that cycle[12].

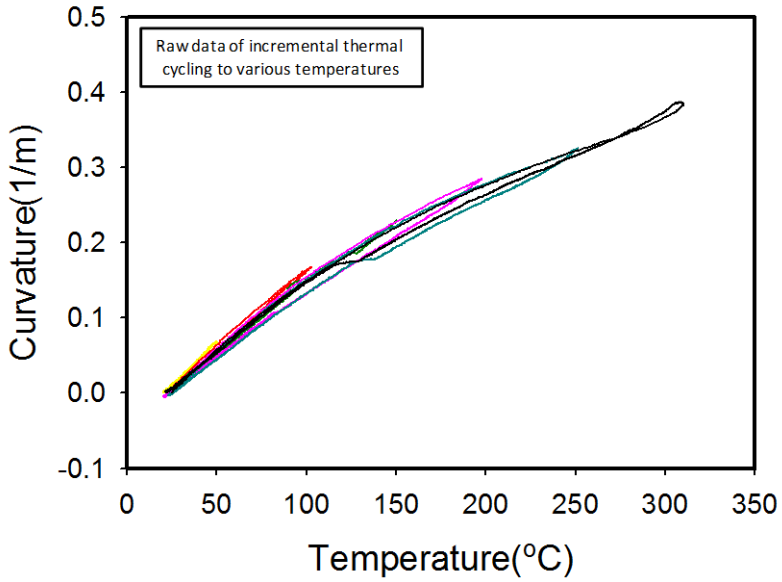

Figure 6-1: The curvature temperature response of coating with varying set-point temperatures. For each temperature range coatings were subjected to three heat cycles. The plot shown here is the data from the second thermal cycling for one of the samples to all the temperature regimes

6.2.1. Evolution of *E*

In Figure 6-2 the elastic modulus did not show any major variations at the various temperatures during either of the thermal cycles in the three coatings. Referring to the results from previous chapter, the slight variations in the values are well within the error range. Except for the case of low-E coating, the *E* values were comparable for the

three cycles for different temperature ranges. This was expected as the calculations for E value utilizes the data only from room temperature till transition temperature which was less than 60 degrees for both the coatings. The E values do not agree with each other for the three cycles of Low-E coating, which can simply be attributed to the higher experimental and computation variability associated with the coating (Chapter-5). One can conclude based on the results that coating elastic modulus does not show any significant variation with maximum temperature change.

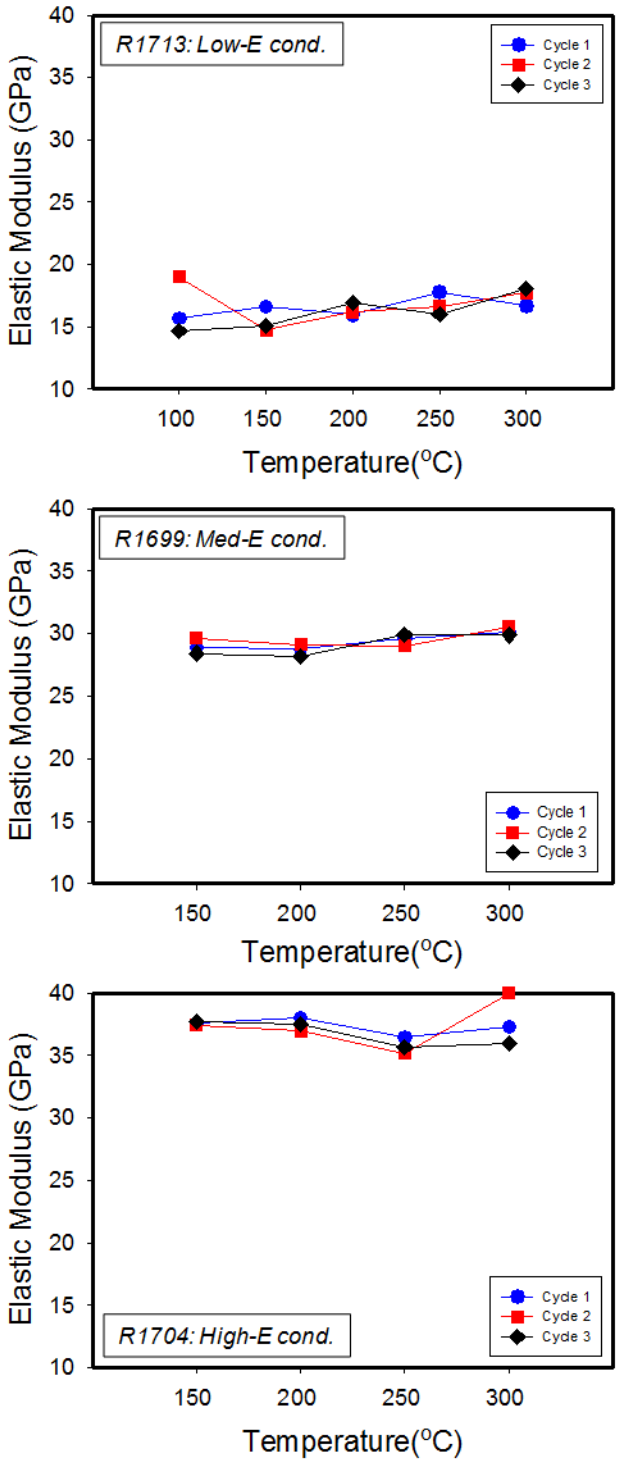

Figure 6-2: The variations in the elastic modulus at different temperature ranges for the coatings sprayed at three different plasma energy conditions

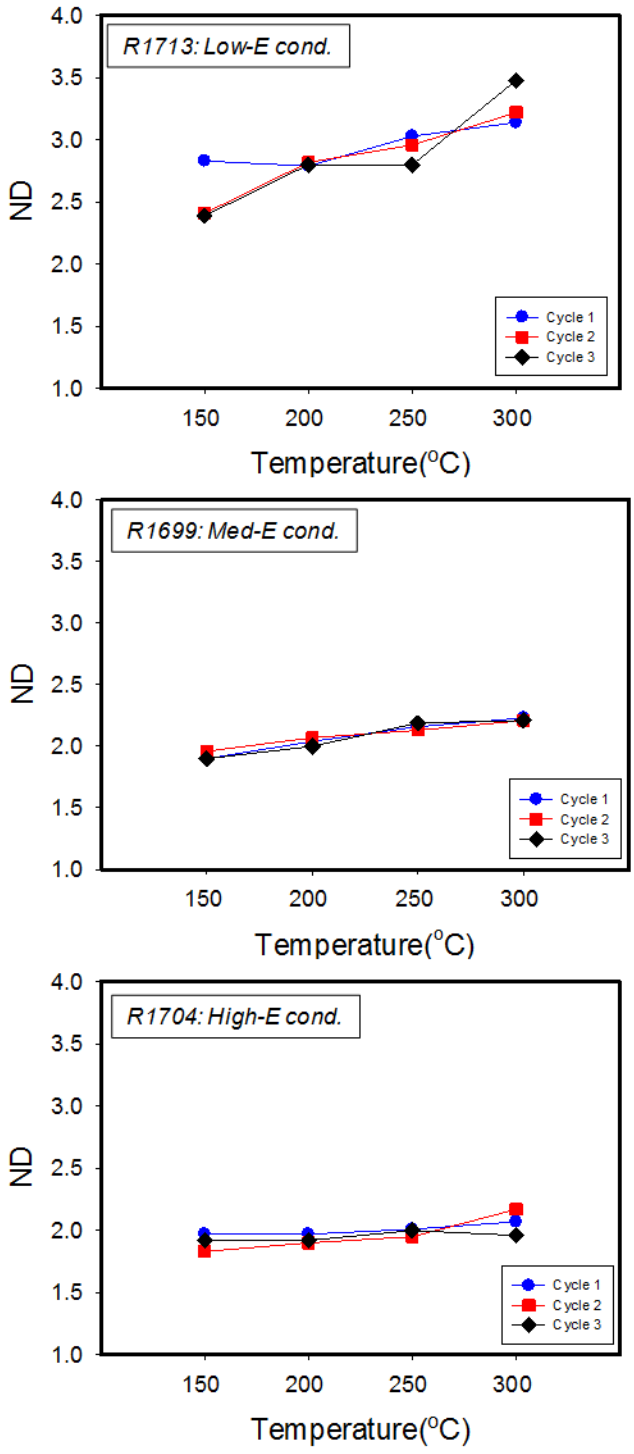

Figure 6-3: The variations in nonlinear degree computed at the various temperatures for the coatings sprayed at three different plasma energy conditions

6.2.2. Evolution of non-linearity (*ND*)

Figure 6-3 presents the results from non-linear analysis of the three coating. It is interesting to observe that the non-linear response of the coating at different temperature ranges were different. As mentioned in chapter-5, the high-E condition coating showed lower non-linearity than the med-E or high-E due to varying defect density. Additionally, the slope of *ND* vs. temperature range curve is higher for the low-E condition coating than med-E followed by high-E. In fact for the high-E coating the slope was almost zero. This indicates that the *ND* evolution rate is dependent on the microstructure of a coating. This can be attributed to two factors: first is that the transition temperature for each coating is different, hence for a given set point temperature the temperature change ($T_{setpoint}$-T_{tr}) for which the coatings will be in its non-linear regime will be larger for the case of low-E condition than other two. This fact along with the presence of larger defect density would cause higher degree of associated defect movement. This attributes to higher *ND* values for increasing set-point temperature. The evolution of *ND* is evident from the slope of the curves in Figure 6-3. Some variations in the trend in low-E condition coating can be attributed to the large measurement variability associated with the coating architecture.

6.2.3. Evolution of hysteresis (*HD*)

As speculated, the hysteresis degree varied as a function of processing condition and temperature. It is essential for a coating to undergo non-linear response to exhibit any hysteresis in the BCT measurement. This implies that hysteresis can be observed only after transition temperature. Since it was different (8.8%, 6.3%, 5.9%) for the three coatings (low-E, Med- E and high-E), the *HD* values are only reported when all of them started showing hysteresis. Figure 6-3 shows the hysteresis degree of the three cycles of

the coating over set-point temperature range from 150 to 300°C. Several observations can be made based on the figure.

For all the three coatings the hysteresis degree was significantly different for the first cycle as compared to the others. Moreover at all the set-point temperature ranges, the *HD* values were similar for the cycle two and three and were also lower than the corresponding first cycle. As mentioned earlier, during cool down process after deposition, ceramic coatings are expected to undergo some additional cracking due to large compressive stresses introduced due to the thermal mismatch. Therefore, during first cycle under BCT measurement, the virgin coating experiences the tensile stresses for the first time and appears to adjust its architecture accordingly for a given strain (temperature) range which might include irreversible movement of some defects. In addition, the possibility of moisture present at defect interfaces can also alter the very first cycle of the day.

Except for the first cycle of low-E condition, all the coatings and their corresponding multiple cycles showed an increase in hysteresis degree till the set point temperature range of 250°C and a drop at 300°C range.. The increase in *HD* numbers with maximum temperature can be explained by the fact that with higher temperature the increase in strain causes higher non-linearity. This means that the extent of defect movement in coatings was increasing with higher temperature, which was able to produce larger hysteresis too. On the other hand, the reason behind the drop in *HD* values at 300°C range is not very clear at this stage however it might be due normalization method adapted for *HD* calculation. To be more specific, the increase in hysteresis area from 250°C to 350°C was not sufficient to produce larger number as compared to previous temperature ranges when divided by the product of curvature and temperature change for that range.

As mentioned earlier, the first cycle of low-E condition coating did not follow the similar trend as the other two, which can be attributed to the larger measurement errors associated with loose (porous) architecture as well as high signal-to-noise ratio of the curvature-temperature response of the coating.

The *HD* evolution was dependent on the coating microstructure. From 150^{o}C to 250^{o}C the change in *HD* was higher for the case of high-E coating (~2.5%) followed by med-E (~1.5%) and low-E coatings (~1%). This can clearly be correlated with the defect density of the coating. On visual inspection it appears that *HD* should be higher for the case of low-E as it has larger hysteresis area for the given temperature range, however when normalized to total curvature and temperature change (definition of *HD*)it shows these results. Figure 6-4 shows a comparison of the coatings' *HD* values of the second cycles for each temperature range. The figure clearly represents not only the difference in absolute values of the *HD*, but also suggests the dependency of *HD* evolution on coating microstructure. The med-E and low-E coatings appear to have almost similar *HD* evolution than high-E condition which shows significantly larger increase in *HD* with temperature. Interestingly, all the coatings (2nd cycle) ended up having similar *HD* at 300^{o}C (~6%), although the reason behind this observation is still unclear. More experiments would be needed to confirm.

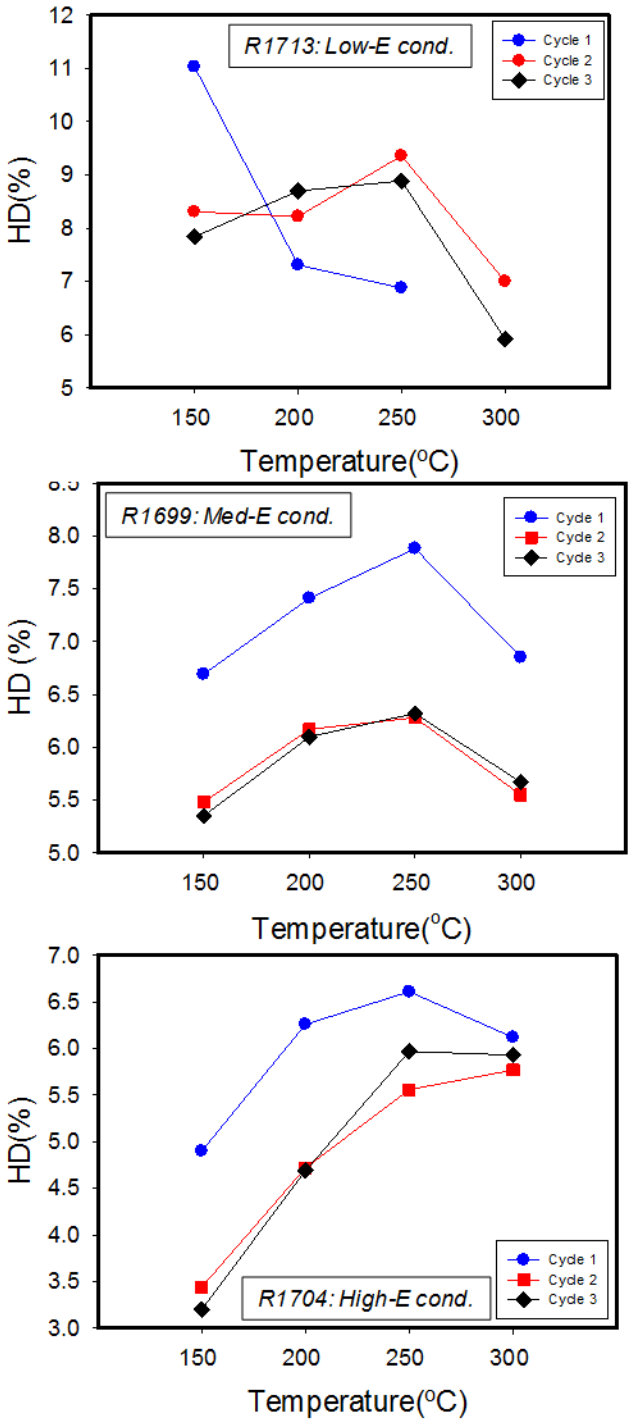

Figure 6-4: The evolution of hysteresis for coatings with temperature. Three coatings sprayed at different plasma energy conditions showed varying trends.

The higher degree of hysteresis observed in the first cycle could be attributed to the presence of moisture in the first cycle. The presence of moisture at the crack interfaces causes the sliding to be much better and smoother. At the end of the heating cycle once the moisture would have evaporated and while the coating is returning to the compressive state, there is more energy dissipated during the cooling cycle which is being given off as a larger value in the *HD*.

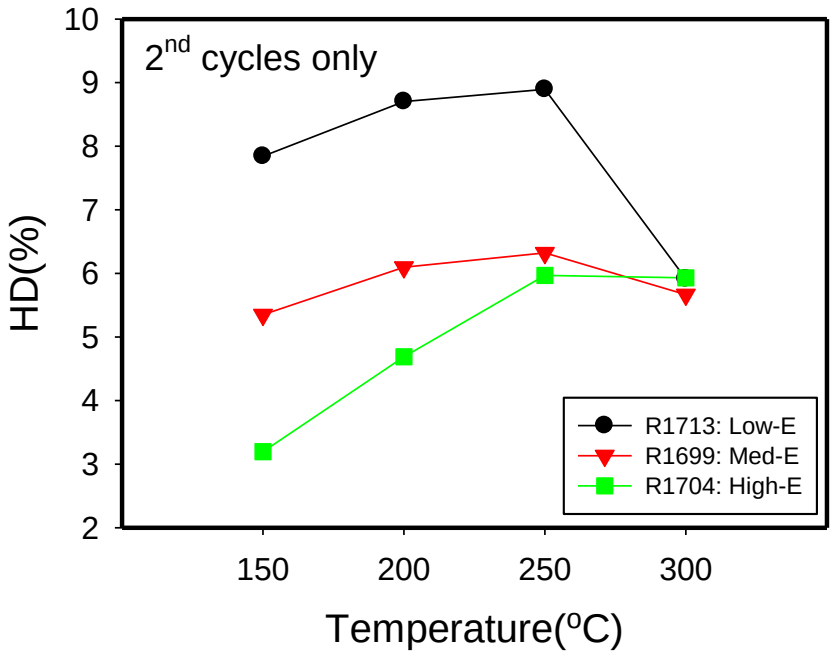

Figure 6-5: Comparison of the hysteresis degree evolution with temperature for the three coatings. Only the second thermal cycle has been considered

From the study carried out it was well established that the anelastic parameter *ND* and *HD* as well as the elastic modulus do vary as a function of the cycling temperature. The variation also followed a trend across the coatings with different levels of porosity produced by three different processing conditions. This means that in addition to the influence of spraying parameters, there was also the influence of the cycling

temperatures for a given sample. Hence while addressing anelastic properties one needs to report them with reference to the temperature range along which it was computed.

7. Deposition Rate Effect on the Anelasticity of Coatings

In previous chapters, we have discussed several aspects of BCT measurement technique and the anelastic parameters. On one hand the error analysis provided a better understanding of possible errors associated with the measurements and quantification, while on the other hand the micro structural sensitivity to the anelastic parameters were observed. Having cemented the basis of the anelastic parameters for three different plasma energy conditions (that were selected to provide significantly different porosity levels to the coatings) we now take a significant step forward. This has been executed by attempting to introduce several processing changes systematically, and to try and analyze the sensitivity of the nonlinear analysis to the various processing parameters. An attempt has been made to quantify these changes in terms of the anelastic parameters.

The properties of the plasma sprayed coatings can be controlled by the defect architecture in coatings which can be tailored by various processing conditions. Starting from the plasma, one could tune the plasma power to achieve different coating microstructure as done in the previous chapters. With changes in the plasma power the enthalpy of the plume changes which results in different extents of particle melting. Under high plasma energy condition the particles would melt more than they would in low plasma energy conditions. The morphology and size distribution of feedstock powder also plays a very important role in the coating architecture. A hollow particle as

in the case of HOSP would provide us better melting and hence a denser coating than the regular fused and crushed particles of zirconia. Moreover, the powder size also has a significant influence on the coatings being sprayed. The amount of heat required to melt a larger particle would be more than that required for a relatively smaller particle which will dictate the molten state and momentum of the particles in plume. All the above stated are termed as the Particle State Parameters (PSP). Hence variations in the PSP can bring about significant changes to the coatings.

There are also other kinds of spraying parameters that can be changed to produce different microstructure, e.g. the spray angle, torch traverse speed, spray distance, feed rate, deposition temperature etc. Each of these has their own influence on the coating. For instance an increase in spray distance would mean that particles need to travel a longer distance in the plume before approaching the substrate. The increase in dwell time of the particles could result in better melting; however the possibility of decrease in particle temperature before depositing on the substrate needs to be accounted for. The powder feed rate as well as the substrate temperature are the parameters which influence the microstructure evolution mechanism. A higher feed rate would create a scenario with smaller time interval between two splats. On the other hand, if the substrate is being preheated, then the coating deposition takes place at an elevated temperature. This leads to better particle – substrate adhesion. These parameters are referred to as Non Particle State Parameters (NPSP). Thus both the PSPs as well as the NPSP have an influence on the architecture of the coating produced. In this chapter of the thesis we would be focusing on some of the Non Particle State Parameters and in particular the powder feed rate (FR), raster speed (RS) and spray distance (SD)..

All the three parameters, FR, RS and SD, can conjointly be considered as the parameters which affect the overall coating deposition rate (DR). The deposition rate of

the particles is calculated as the ratio of powder feed rate to the relative speed between the plasma torch and substrate. Variations in these things can significantly influence the manner in which the particles deposit and form the ultimate coating structure. The manner and the rate at which the tensile quenching stresses are released by internal cracking of coating play a crucial role in the evolution of the final coating architecture. If the particles were to be quenched rapidly then the chances of localized architectural defects to be formed is high. The study has mainly focused on the anelasticity change due to change in DR. Figure 7-1 shows the schematics of high and low DR conditions.

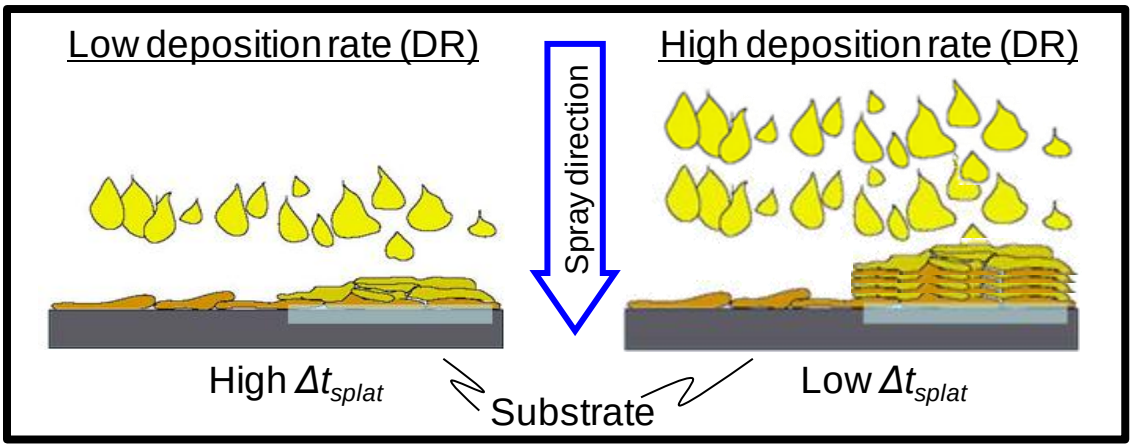

Figure 7-1: Representation of snapshot of schematics of the two conditions with low and high Δt_{splat}. It can be observed that the low Δt_{splat} will produce a coating with higher thickness per pass. (Diagram courtesy Dr. Kentaro Shinoda and Dr. Alfredo Valarezo).

7.1. Influence of varying splat interval

Prior to the discussion of results obtained from this study, it is important to understand a parameter called, splat interval (Δt_{splat}), which can be defined as the time interval between two consecutive splats. For instance, let us assume that all the particles are in similar melting state, then if the Δt_{splat} is small, the columnar grain growth may

continue from a previously deposited splat through the successive splat leading the structure to a good cohesive strength. On the other hand in the case of large Δt_{splat}, it may be possible that the successive splat is coming in contact with a fully solidified splat. There are many stages in the solidification of a splat. The stage during which an incoming splat comes in contact with a solidifying splat governs the coating microstructure. This time interval is influenced by Δt_{splat}. The Δt_{splat} can be changed by changing the torch raster speed (RS) as well as feed rate (FR). Figure 7-2 presents the relationship between splat interval and DR changed by FR and RS.

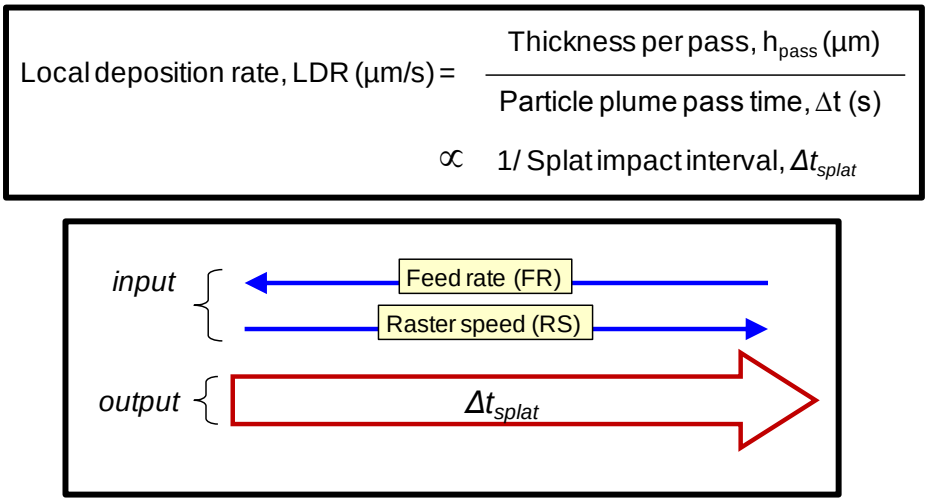

Figure 7-2: The relationship between deposition rate and the processing parameters such as powder feed rate and torch raster speed

There are other factors and mechanisms associated high DR which cannot be ignored. For example, quenching of plasma with high federate may lower the plasma enthalpy resulting in lower melting of particles. Moreover, high DR will impart high thermal energy to substrate which can increase substrate temperature resulting in better flattening of splats and hence better cohesive strength. One should consider these side effects to understand the DR effect on coating microstructure evolution.

As mentioned earlier, the coating microstructure strongly depends on particles' melting state, which can be altered by changing plasma energy or by changing particle dwell time in plasma via spray distance. Therefore, it would be interesting to investigate the effect of spray distance (particle dwell time in plasma plume) along with FR and RS on coating microstructure. The study conducted in this chapter shows results on the combined effect of spray distance and deposition rate. Since the anelastic parameters of coatings are sensitive to coating microstructure, the changes introduced to coating can be captured utilizing these parameters. The BCT technique has been used to exploit these differences among the coatings in an attempt to characterize as well as tailor them by changing the deposition rate of the particles.

7.2. Design of Experiment

Figure 7-3 shows the summary of experimental design adopted for the study. YSZ powder was used to spray 2 sets of coatings at 100mm and 150mm spray distance. For each spray distance, three raster speeds were used for the robot at 333mm/sec, 500mm/sec and 1000mm/sec. Additionally for each of these raster speeds, four powders feed rates of 15, 30, 45 and 60g/min were used. Each of these coatings was sprayed on a 9''X1'' aluminum beam mounted on In-situ Coating Property sensor (ICP). Measurements from ICP were utilized to obtain evolving stress of coating during deposition. The deposited coatings, later, were subjected to thermal cycling using BCT setup, and the data was analyzed to compute anelastic parameters of coatings. In addition, SEM micrographs were taken for selective coatings for their micro-structural evaluation.

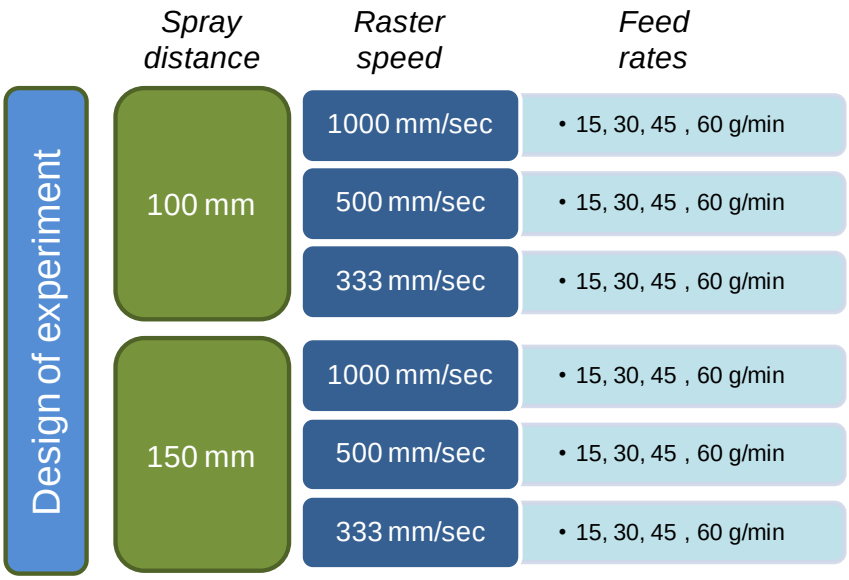

Figure 7-3: Design of experiments by varying multiple processing parameters such as Spray Distance, Raster Speed, and Feed Rate.

7.3. Results and Discussions

Figure 7-4 shows the results obtained after the nonlinear analysis on the coatings sprayed at 100 mm standoff distance.

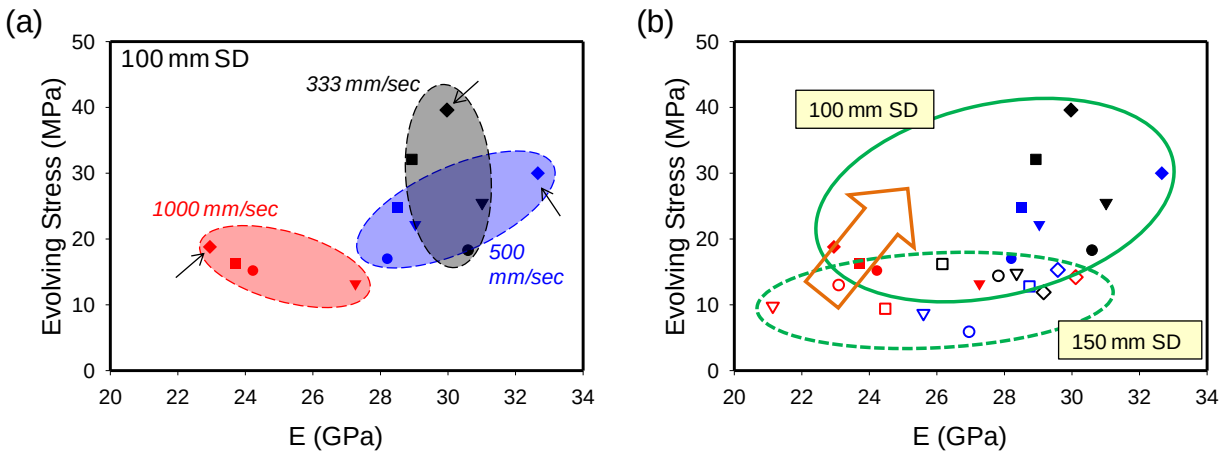

Figure 7-4: (a) Plot of evolving stress and elastic modulus for the coatings sprayed at 100mm spray distance. Coatings sprayed at different traverse speeds occupied different zones in the map. (b)The shift in the zone of coatings on a evolving stress vs. elastic modulus plot when sprayed at 100mm spray distance and 150mm spray distance

The coatings sprayed at 333mm/sec and 500mm/sec raster speeds were appear to overlap each other in the plot of evolving stress vs. elastic modulus (Figure 7-4 (a)). Though the difference in traverse speed of the robot could have introduced changes in the coating architecture, from the figure, it suggests that the coatings of both those spray conditions can be considered to have a similar architecture. We do understand that during coating deposition rapid quenching of the particles takes place and that this generates a lot of localized stresses (evolving stress) in the system. If this phenomenon of very high localized stresses were to be prolonged, then the value of evolving stresses would increase with decreasing raster speed. . At slower raster speeds, the plasma plume spends more time on each given area of the substrate thereby causing very high evolving stresses. The effect is more pronounced in the case of higher powder feed rates when more particles are being thrust on the substrate as seen in the Figure 7-4(a). (The arrows indicate the 60 g/min condition).

The effect of lower raster speeds has its own advantages as far as deposition efficiency is concerned. At lower raster speeds, the amount of material (powder) deposited would be more. Moreover since the local substrate deposition temperatures would be higher, it would result in better flattening of splat, higher deposition efficiency and hence a much denser coating. Thus coating deposited under such circumstances tends to have lesser defect density and would exhibit a higher value of elastic modulus. This clearly explains the position of these coatings on the right - top position on Figure 7-4 (a). However with a significant increase in the raster speed, the splat interval Δt_{splat} may increase considerably. As discussed before, such a change induces significant variations in the defects' architecture in the coating which explains the different zone for these coatings on the evolving stress-elastic modulus map The high raster speed condition would introduce large Δt_{splat} which would result in a coating with poor inter-splat bonding, and hence lower evolving stress as well as elastic modulus. Therefore the coatings with 1000 mm/sec raster speed occupy the lower left corner on Figure 7-4(a).

Figure 7-4 (b) indicates the trend of evolving stress and elastic modulus between the coatings sprayed at 100mm and 150mm spray distance. With an increase in spray distance (150mm) the particles will have a larger dwell time in the plume, which in turn would increase However since the particles need to travel a larger distance before depositing on the substrate there exists a possibility of an in-flight temperature drop as they move further away from the torch, which can result in some degree of re-solidification of molten particles before deposition. As mentioned earlier, the presence of such partially unmolten particles contribute to an increase in the overall defect density of the coatings[12]. This result in a lower elastic modulus for such coatings due to the lack of sufficient density. When sprayed at a larger spray distance the particles also

experience a slight decrease in their impact velocity. Such decreased impact velocity coupled with the effect of decreased particle temperatures upon contact with the substrate results in lower evolving stresses for such coatings. Therefore, the coatings sprayed at 150mm occupy a region of low elastic modulus as well as low evolving stress in Figure 7-4 (b). At a reduced spray distance of 100mm there is an upward shift in the zone on the evolving stress vs. elastic modulus graph confirming the presence of lesser defect density as well as higher localized quenching rates for such coatings.

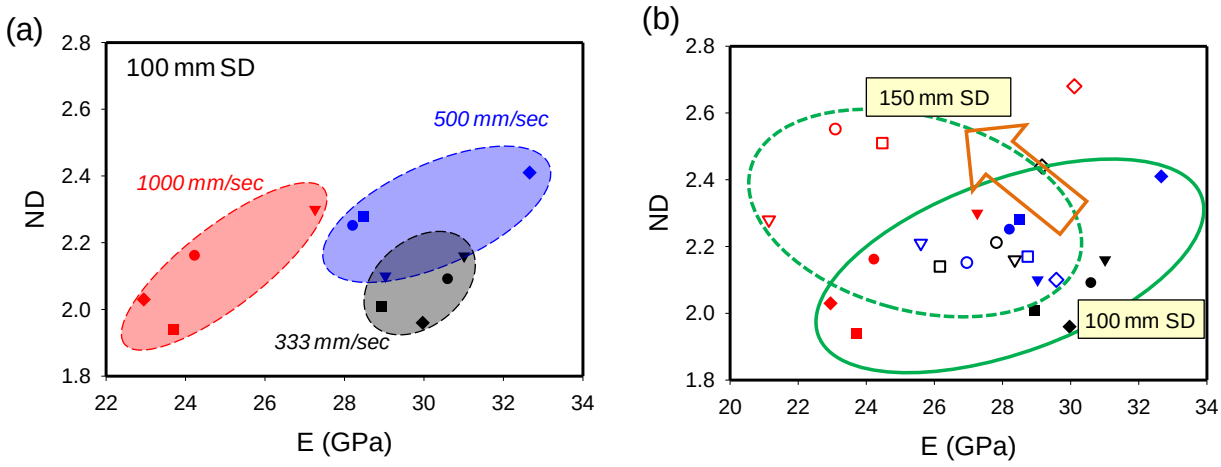

Figure 7-5: (a) Plot indicating the variations in nonlinear degree and elastic modulus for coatings sprayed at different raster speeds. (b) Comparative study between the coatings sprayed at 100mm and 150mm spray distance in terms of their nonlinearity

The variations in the coatings sprayed at 100mm and 150mm can also be characterized in terms of their nonlinearity. Figure 7-5(a) shows a plot of nonlinear degree and elastic modulus for 100 mm spray distance .As mentioned earlier, since lower raster speeds result in lower Δt_{splat}, they produced a lesser defect density and a good inter-splat bonding. Therefore, the coatings exhibited a high elastic modulus and limited non-linear degree. The comparable non-linear parameters of the coatings

sprayed at 500mm/sec and 333mm/sec can be attributed to their comparable defect architectures. These interpretations can further be validated by the SEM micrographs of a few selected coatings shown in Figure 7-6. The results from SEM indicate that the level of porosity at 333mm/sec as well as 500mm/sec does not seem to be very different. The similarity in coating architecture is being reflected in the results of the nonlinear analysis on these coatings. The coatings sprayed at 1000mm/sec raters speed would have caused a lot more defect density due to high Δt_{splat} as explained before, hence in Figure 7-5(a) the red region was expected to contain at a higher value of *ND*. However, the trend is somewhat opposite to this hypothesis. It is possible that beyond a certain increase in raster speeds the porosity in coatings do not increase, however further investigation is needed to make any conclusions on this.

Figure 7-5(b) represents the shift in the nonlinear parameters for coatings sprayed at 150mm spray distance, similar to what was observed in Figure 7-4(b). The presence of higher degree of partially molten particles at 150mm SD causes the coatings to exhibit a higher degree of nonlinearity and a relatively lower elastic modulus. At 150mm SD one observes that for the highest raster speed of 1000mm/sec (hollow red points) the effect of increased defect density is more prominent. This further creates curiosity as to why a similar trend was not observed in the case of the 100 mm SD coatings.

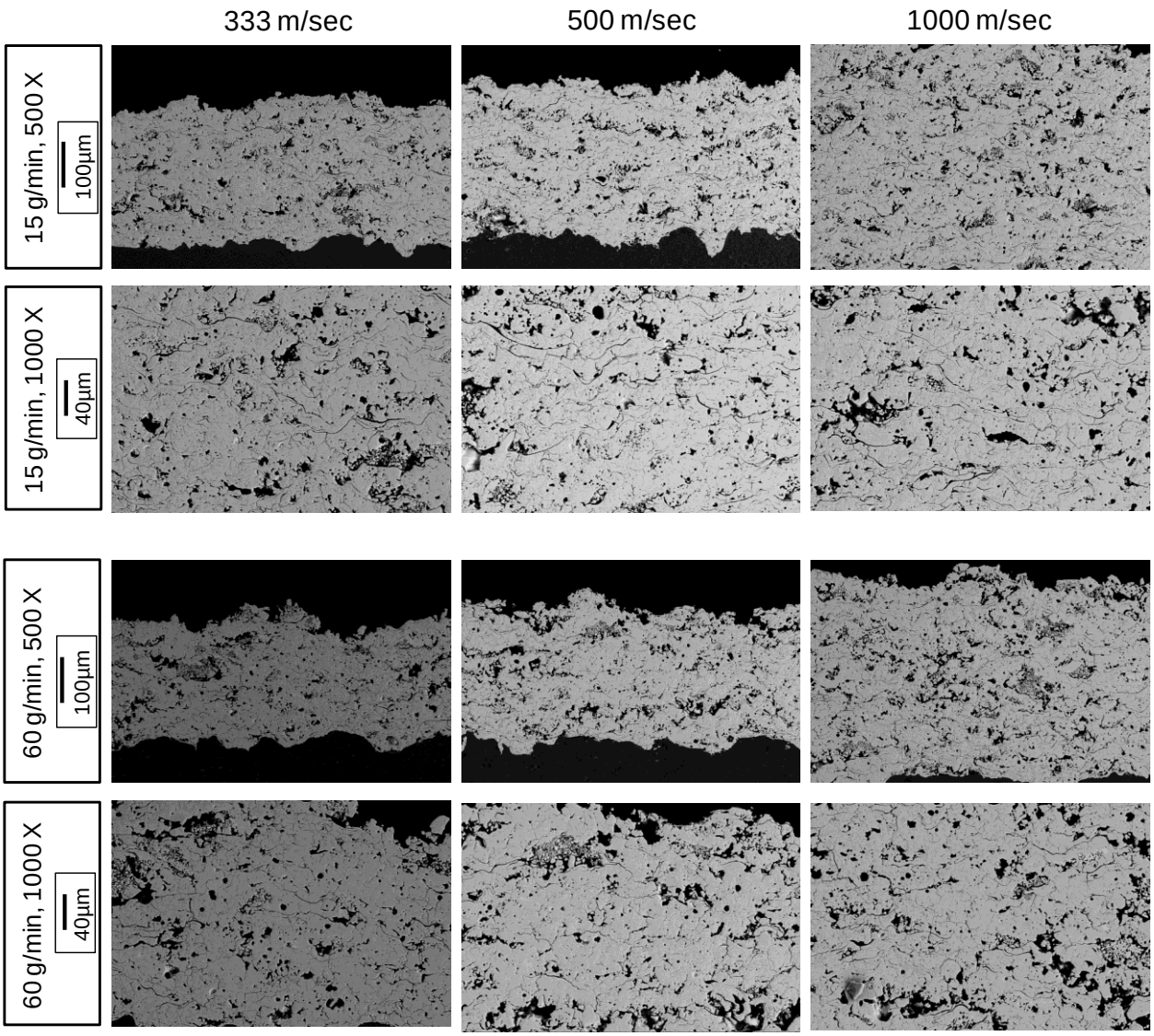

Figure 7-6: SEM images of the coatings sprayed at three different raster speeds. Only extreme conditions for feed rate (15 and 60g/min) are shown here. All of these are coatings sprayed at 100mm spray distance

Figure 7-7 presents a detailed map of the anelastic properties (*E, ND* and *HD*) of these coatings over a 3D space. Some interesting patterns can be observed in the figure. The coatings with deposited with high raster speed exhibited higher hysteresis degree as compared to those sprayed with lower raster speed. This can be attributed to the

lower Δt_{splat} associated with high raster speeds which in turn provide higher degree of defect interfaces thereby causing significant frictional sliding during the BCT measurement. The presence of higher number of defect interfaces with 1000mm/sec raster speed case can also observed in the SEM micrographs (Figure 7-6). Coatings with moderate raster speed exhibited slightly higher *HD* than those with low raster speed (333 mm/sec) due to higher Δt_{splat} with 500 mm/sec. However, with these two raster speed the changes are not as significant as it was with 1000 mm/sec, which can be because of lesser difference in raster speeds between moderate and low raster speed cases.

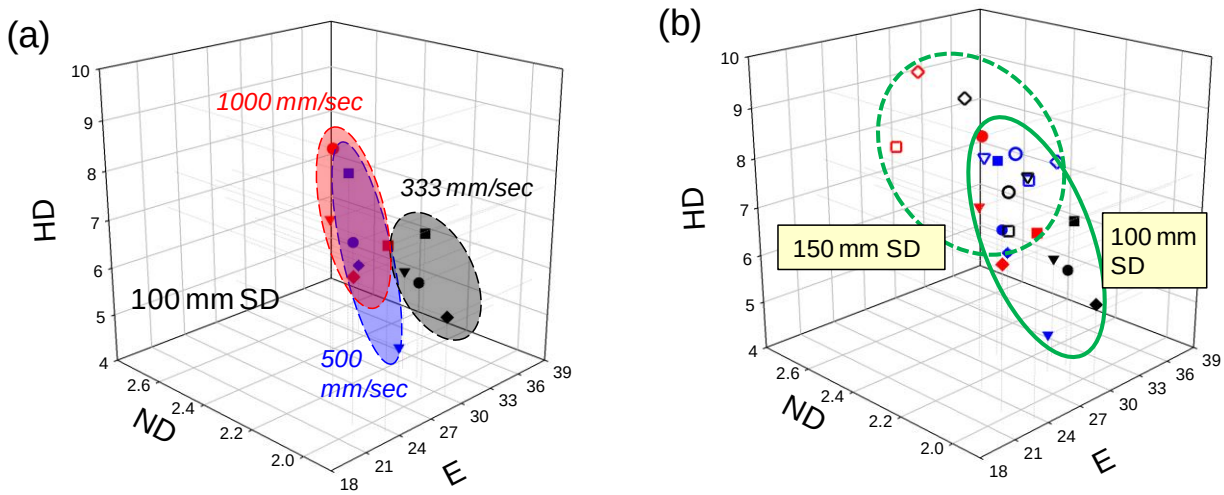

Figure 7-7: (a) variation of anelastic parameters for coatings sprayed at different raster speeds.(b) variations between the two spray distances 100 and 150mm.

Between the 100mm and 150mm SD the differences are more pronounced, and the latter clearly shows a shift towards a zone of higher *ND* and *HD* as show in Figure 7-7(b) . This fortifies our hypothesis on the increase in defect density in the form of splat interfaces as well as cracks and pores. The higher values of elastic modulus and relatively lower position in the anelastic zone of 100 mm SD coatings is explained by the

better inter splat bonding as well as lower defect density due to higher melting of particles.

In this study, the nonlinearity as well as anelasticity of coatings were measured using the BCT technique and their sensitivity to the various changes in the processing conditions were analyzed. Changes in parameters such as spray distances, powder feed rate and raster speeds were deliberately brought about to bring about changes in the defect architecture. Except for the case of 100mm spray distance and raster speed of 1000mm/sec, the coatings sprayed at all other conditions showed convincing results in terms of their anelastic parameters. It was observed that the change in spray distance from 100mm to 150mm had larger effect on overall change in coatings' anelasticity. For 100mm spray distance case, the anelasticity was significantly affected by changing the raster speed from 500 and 333mm/sec to 1000mm/sec due to larger difference in numbers. Hence the fact that BCT technique can be used as a potential tool to establish and quantify architectural changes in coatings has been well established.

8. Summary and Future Work

Plasma sprayed ceramic coatings exhibit novel anelastic mechanical behavior, which was the main focus of this thesis. Being governed by the coating's architecture, this behavior is very unique and can be utilized to compare coatings. The bi-layer curvature-temperature (BCT) measurement technique was used to measure and characterize the anelastic behavior of coatings. The higher fidelity of BCT measurement compared to other property measurement techniques was utilized to address the variability among coatings processed at different conditions. Beginning with the understanding that the anelastic properties of a coating are a function of the coatings' microstructure, an attempt has been made to bring about systematic variations in these parameters from the processing front. An effort was made to investigate the evolution of anelastic parameters at different stages of strain. Through an exhaustive experimental design, the correlation of process parameters with the anelastic parameters was investigated.

The first study discussed in this thesis, was conducted to evaluate the possible errors and their sources associated with the BCT measurement and quantification. Both experimental and computational variability were evaluated for the error span of measured data and computed values. Three coatings with significantly different microstructures were prepared for this analysis. It was observed that the coating with high porosity level responded with higher variability in its BCT measurement over multiple cycles as compared to those with lower porosity level. The variability was captured by the quantified non-linear parameters of the coatings, and they showed

higher dispersion for the case of lower porosity coating. In addition to experimental error, the error analysis was also conducted on the cases with deliberately introduced errors in the input parameters of the non-linear analysis program, such as coating and substrate thicknesses and transition temperature. The results suggested that the non-linear parameters of BCT measurement were very sensitive to the input parameters. Elastic modulus showed strong dependence on coating and substrate thicknesses. However the non-linear parameters did not exhibit any significant change with errors in the thicknesses. The sensitivity of the transition temperature to the anelastic parameters was very limited. This study suggested that one has to have an estimate of porosity level in coatings as well as the possible input errors while interpreting the anelastic parameters as coating property evaluation.

Having obtained a degree of confidence on the error ranges of the BCT measurement technique, the evolution of the anelastic parameters was examined by computing them at different temperature regimes. For the coatings to exhibit nonlinearity it is essential for the defects present in them to get activated. The extents of mobility of these defects as well as the zone of transition temperatures vary with the defect densities in coatings. Hence this study focused on coatings with three different porosity levels and characterized them at different temperature ranges. Since the activation of defects in the coating is a temperature dependent(and hence strain dependent) function, the anelastic properties obtained at different temperatures were analyzed. It was observed that for all the coatings the evolution of the three anelastic parameters (*E*, *ND* and *HD*) showed a systematic pattern. For each coating, their *E* values remained constant with increasing temperature range due to their computation below transition temperatures. On the other hand, the *ND* and *HD* values appeared to be increasing with higher temperature ranges. Moreover, their evolution rate was

higher with higher porosity level, which was attributed to higher defect density participating in anelastic phenomenon.

The last chapter of this thesis is a comprehensive processing study to closely monitor the anleastic properties to predefined changes in spraying parameters. Systematic study was conducted where in the processing parameters were changed in increments significant enough to bring about a change in the coatings' nonlinear properties. Changes with the powder feed rates, spray distances, raster speeds were quantified and analyzed. The result suggested that the effect of a smaller change in raster speed (as in the case of 333mm/sec and 500mm/sec) versus a much larger increment (1000mm/sec) appeared to be limited on the evolving stress as well as anelastic parameters in the former case. Moreover the low and high magnification SEM micrographs of the coatings showed a similar trend; the coatings with less difference in raster speeds (333 and 500mm/sec) exhibited significantly similar microstructure as compared to the coating with 1000 mm/sec. In addition, the creation of larger defect densities at higher spray distance was confirmed not merely on the basis of the elastic modulus but also with the anleastic parameters *ND* and *HD*. This was attributed to the better melting and KE of particles with 100 mm spray distance. It is therefore imperative to take cognizance of these essential factors for one to estimate the influence of the processing parameters to the coating anelasticity.

The results obtained in this study provide a better understanding and interpretation of anelasticity of coatings. All the measurements conducted in this work involved low temperature thermal cycling of coatings. However, in future, it would be interesting to observe the behavior of these micro-structural features at a much higher and dynamic strain rates to match the actual service temperature of TBCs application. From the understanding of anelascitiy developed in past, it is safe to assume that the mechanism

of relative movements of defects surfaces would be similar even at higher temperature. While the higher temperature and loading rates may influence the anelastic properties, the dependency of thermal conductivity of the system during such cyclic tests could also be analyzed in order to better understand the behavior of these defects. Such strain rate dependent thermal conductivity study could complement the present research as well as lay the foundation for the future. After subjecting the system to a certain number of cycles (as it would in the actual application) there could be a possibility that the coating starts behaving even more compliant, then it opens up a whole new dimension of research to venture out into. Whether or not the interfacial roughness is lost under such conditions would be an academically interesting as well as an industrially relevant topic to be probed.

References

1. H. Herman, S. Sampath, and R. McCune, Thermal spray: Current status and future trends, *Mrs Bulletin*, 2000, **25**(7), p. 17-25.

2. S. Sampath, Thermal sprayed ceramic coatings: fundamental issues and application considerations, *International Journal of Materials & Product Technology*, 2009, **35**(3-4), p. 425-448.

3. H. Herman, and N.R. Shankar, Fundamental-Aspects of Thermal Barrier Coatings, *American Ceramic Society Bulletin*, 1984, **63**(12), p. 1475-1475.

4. M. Peters, C. Leyens, U. Schulz, and W.A. Kaysser, EB-PVD thermal barrier coatings for aeroengines and gas turbines, *Advanced Engineering Materials*, 2001, **3**(4), p. 193-204.

5. J.B. Walsh, Effect of Cracks on Uniaxial Elastic Compression of Rocks, *Journal of Geophysical Research*, 1965, **70**(2).

6. D.R. Clarke, and C.G. Levi, Materials design for the next generation thermal barrier coatings, *Annual Review of Materials Research*, 2003, **33,** p. 383-417.

7. L.B. Chen, Yttria-stabilized zirconia thermal barrier coatings - A review, *Surface Review and Letters*, 2006, **13**(5), p. 535-544.

8. N.P. Padture, M. Gell, and E.H. Jordan, Materials science - Thermal barrier coatings for gas-turbine engine apptications, *Science*, 2002, **296**(5566), p. 280-284.

9. P. Fauchais, Understanding plasma spraying, *Journal of Physics D-Applied Physics*, 2004, **37**(9), p. R86-R108.

10. S. Ben Naoua, M. El Ganaoui, H. Sammouda, and P. Fauchais, Raped solidefication study of stabilized zirconia under plasma spraying, *High Temperature Material Processes*, 2006, **10**(2), p. 185-196.

11. S. Sampath, and H. Herman, Plasma Spray Forming Metals, Intermetallics, and Composites, *Jom-Journal of the Minerals Metals & Materials Society*, 1993, **45**(7), p. 42-49.

12. G. Dwivedi, "On the anelastic behavior of plasma sprayed ceramic coatings: Observations, Characterizations and Application," Stony Brook University.

13. C. Zener, Anelasticity of Metals, *T Am I Min Met Eng*, 1946, **167**, p. 155-191.

14. L. Li, A. Vaidya, S. Sampath, H.B. Xiong, and L.L. Zheng, Particle characterization and splat formation of plasma sprayed zirconia, *Journal of Thermal Spray Technology*, 2006, **15**(1), p. 97-105.

15. G.E. Dieter, Mechanical Metallurgy, *Mc-Graw Hill series in Materials Science and Engineering*, Mc-Graw Hill, 1988.

16. Y.J. Liu, T. Nakamura, G. Dwivedi, A. Valarezo, and S. Sampath, Anelastic Behavior of Plasma-Sprayed Zirconia Coatings, *Journal of the American Ceramic Society*, 2008, **91**(12), p. 4036-4043.

17. H.B. Xiong, L.L. Zheng, L. Li, and A. Vaidya, Melting and oxidation behavior of in-flight particles in plasma spray process, *International Journal of Heat and Mass Transfer*, 2005, **48**(25-26), p. 5121-5133.

18. A. Vaidya, T. Streibl, L. Li, S. Sampath, O. Kovarik, and R. Greenlaw, An integrated study of thermal spray process-structure-property correlations: A case study for plasma sprayed molybdenum coatings, *Materials Science and Engineering a-Structural Materials Properties Microstructure and Processing*, 2005, **403**(1-2), p. 191-204.

19. S. Kuroda, and T.W. Clyne, The Quenching Stress in Thermally Sprayed Coatings, *Thin Solid Films*, 1991, **200**(1), p. 49-66.

20. V. Arnault, R. Mevrel, S. Alperine, and Y. Jaslier, Thermal barrier coatings for aircraft turbine airfoils : thermal challenge and materials, *Revue De Metallurgie-Cahiers D Informations Techniques*, 1999, **96**(5), p. 585-597.

21. S. Sampath, X.Y. Jiang, J. Matejicek, L. Prchlik, A. Kulkarni, and A. Vaidya, Role of thermal spray processing method on the microstructure, residual stress and properties of coatings: an integrated study for Ni-5 wt.%Al bond coats, *Materials Science and Engineering a-Structural Materials Properties Microstructure and Processing*, 2004, **364**(1-2), p. 216-231.

22. T. Nakamura, and Z. Wang, Simulations of crack propagation in porous materials, *Journal of Applied Mechanics-Transactions of the Asme*, 2001, **68**(2), p. 242-251.

23. S. Sampath, and H. Herman, Rapid solidification and microstructure development during plasma spray deposition, *Journal of Thermal Spray Technology*, 1996, **5**(4), p. 445-456.

24. A. Kulkarni, A. Vaidya, A. Goland, S. Sampath, and H. Herman, Processing effects on porosity-property correlations in plasma sprayed yttria-stabilized zirconia coatings, *Materials Science and Engineering a-Structural Materials Properties Microstructure and Processing*, 2003, **359**(1-2), p. 100-111.

25. B.W. J., and M.R. A., TBCs for Better Engine Efficiency, *Advance Materials and Processing*, 1989, **8**, p. 29-33.

26. T. Nakamura, and Y.J. Liu, Determination of nonlinear properties of thermal sprayed ceramic coatings via inverse analysis, *International Journal of Solids and Structures*, 2007, **44**(6), p. 1990-2009.

27. Y. Liu, T. Nakamura, V. Srinivasan, A. Vaidya, A. Gouldstone, and S. Sampath, Non-linear elastic properties of plasma-sprayed zirconia coatings and associated relationships with processing conditions, *Acta Materialia*, 2007, **55**(14), p. 4667-4678.

28. E.F. Rejda, D.F. Socie, and T. Itoh, Deformation behavior of plasma-sprayed thick thermal barrier coatings, *Surface & Coatings Technology*, 1999, **113**(3), p. 218-226.

29. S.R. Choi, D.M. Zhu, and R.A. Miller, Mechanical properties/database of plasma-sprayed ZrO2-8wt% Y2O3 thermal barrier coatings, *International Journal of Applied Ceramic Technology*, 2004, **1**(4), p. 330-342.

30. J. Matejicek, and S. Sampath, In situ measurement of residual stresses and elastic moduli in thermal sprayed coatings - Part 1: apparatus and analysis, *Acta Materialia*, 2003, **51**(3), p. 863-872.

31. J. Matejicek, S. Sampath, D. Gilmore, and R. Neiser, In situ measurement of residual stresses and elastic moduli in thermal sprayed coatings - Part 2: processing effects on properties of Mo coatings, *Acta Materialia*, 2003, **51**(3), p. 873-885.

32. S. Sampath, V. Srinivasan, A. Valarezo, A. Vaidya, and T. Streibl, Sensing, Control, and In Situ Measurement of Coating Properties: An Integrated Approach Toward Establishing Process-Property Correlations, *Journal of Thermal Spray Technology*, 2009, **18**(2), p. 243-255184.

33. Y.C. Tsui, and T.W. Clyne, An analytical model for predicting residual stresses in progressively deposited coatings .1. Planar geometry, *Thin Solid Films*, 1997, **306**(1), p. 23-33.

34. G. Dwivedi, T. Wentz, S. Sampath, and T. Nakamura, Assessing Process and Coating Reliability Through Monitoring of Process and Design Relevant Coating Properties, *Journal of Thermal Spray Technology*, 2009.

35. G. Dwivedi, T. Nakamura, and S. Sampath, Controlled Introduction of Anelasticity in Plasma-Sprayed Ceramics, *Journal of the American Ceramic Society*, 2011.